THIRD QUARTERLY PROGRESS REPORT

PERIOD ENDING MARCH 31, 1965

RESEARCH & DEVELOPMENT
ON
FUEL CELL SYSTEMS

Contract No.   NAS 8-2696

N65-23276

Prepared for:

National Aeronautics and Space Administration
George C. Marshall Space Flight Center
Huntsville, Alabama 35812

ALLIS-CHALMERS

RESEARCH DIVISION

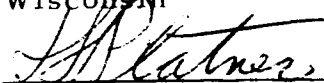MILWAUKEE, WISCONSIN 53201

APRIL 26, 1965

RESEARCH AND DEVELOPMENT

ON

FUEL CELL SYSTEMS

Third Quarterly Progress Report
Under Modification Number 6, Contract NAS 8-2696
For the Period Ending March 31, 1965

Prepared for

National Aeronautics and Space Administration
George C. Marshall Space Flight Center
Huntsville, Alabama

Research Division, Department 3341
Allis-Chalmers Manufacturing Company
Milwaukee, Wisconsin

Approved: _J. H. Platner_

J. L. Platner
Program Manager

TABLE OF CONTENTS

FOREWORD

This is the third quarterly report submitted after Modification Number 6 to Contract Number NAS 8-2696. The report covers the technical progress of "Research and Development on Fuel Cell Systems" for the period of January 1, 1965 to March 31, 1965.

Work under this contract is being performed by the Research Division of Allis-Chalmers Manufacturing Company, Milwaukee, Wisconsin. Mr. R. M. Casper, Vice President, is the Director of Research. Dr. Powell A. Joyner is the General Manager of the Space and Defense Sciences Department of the Research Division. A project type organization was formed to carryout the program specified in the contract. J. L. Platner, Program Manager, has direct responsibility for the management and technical aspects of the program. Program management includes: D. P. Ghere, Assistant Program Manager; Dr. J. R. Hurley, Manager, Systems Research and Development; P. D. Hess, Manager, Engineering; R. E. Lochen, Manager, Fabrication and Testing; C. R. Martin, Manager Quality Assurance; Gunnar Johnson, Manager, Business Administration; and, M. J. Knuijt, Program Planner.

SUMMARY

Work being performed under the terms of this contract is divided into the following three major tasks:

Part I Tasks   -   Research and Technology

Part II Tasks -   Breadboard and Experimental Items

Part III Tasks - System Test Models

Part I Tasks   -   Under this part of the contract work is being performed to advance the art of fuel cells in general, and specifically, to support the work being performed under Part II and III Tasks. During this report period the following conclusions were reached, based on the analysis of test programs completed or in progress.

(a)   A mathematical evaluation of several plate designs resulted in the selection of a design which reduced the voltage drop per cell 8 to 10 millivolts. Trade-offs between the added weight and the increased cell efficiency were also analyzed.

(b)   An analysis of a typical "in-duct" heater arrangement was made using the thermal analysis computer program. Initial runs of this program have established the feasibility of this arrangement and its operating paramaters.

(c)   Design criteria for a static condenser-separator water recovery device have been established, based on a mathematical analysis.

(d)   A study of water acceptability monitors has resulted in the selection of two methods (direct pH measurement and ionic conductivity) for further study.

(e)   Further control studies have established that a proportional-derivative control system will maintain the temperature of the fuel cell within the established limits without any inherent instability provided a proper choice is made for the values of proportional sensitivity and derivative time. The limits for these values have also been established.

(f)   A study of reactant gas pressure surges during fuel cell operation has established the frequency and amplitude of the resonant condition. Computer results show that the present designs have a low resonant frequency (15 to 40 cps, with a maximum amplitude of less than 0.03 psi).

PART II TASKS - These tasks cover the evaluation of breadboard models of fuel cell systems built to various base technologies. The following major achievements under this part of the contract have been made:

(a)   The MSC 29 volt, 1.8 KW breadboard system built to August 1964 base technology has completed over 700 hours of operation under load at MSC - Houston. During this period 673 KWH of energy was produced.

(b)   An additional 28 volt, 2.0 KW breadboard system (A-C BB #2) was constructed and is being performance tested. The significant technological advancements in this system resulted in power growth and improved

efficiency in addition to improved electrical performance. To date, 720 hours of operation under load have been logged, and 836 KWH of energy has been produced. The average cell efficiency of A-C BB # 2 was 78 percent compared to 73 percent for the MSC unit.

<u>PART III TASKS</u> - These tasks cover the building of a number of 2 KW fuel cell system models employing advanced technology. The deliverable models will contain flight-designed hardware and will have automatic, self-contained controls.

The first four units (Systems 5 and 2 for in-house testing at Allis-Chalmers, and Systems 3 and 4 for delivery to NASA) are in various stages of fabrication. Hardware components such as pressure regulators, solenoid valves, pressure transducers, etc., have been purchased and received. Design verification testing of these components is in progress.

Development and engineering tests in support of Part III Tasks have lead to the following accomplishments:

(a)   A vibration equivalent model of the fuel cell assembly has been vibration tested at NASA - Huntsville. No failures occurred.

(b)   The redesigned fuel cell plates were performance tested in small test modules. Test results indicate that the performance and moisture removal characteristics of the new design are superior to the previous design.

(c)   Minor modifications in the design of the secondary coolant flow path in a thermal mockup of the fuel cell module have reduced the flow resistance approximately 0.30" H_2O at 55 cfm of helium.

(d) A Water Recovery Subsystem has been evolved. A breadboard model of the system has been feasibility tested.

(e) The Electrical Monitoring and Control, and the Instrumentation Subsystems designs have been completed. Breadboard layouts of these systems have been built and tested. Prototype models of the printed circuit boards for these subsystems are being fabricated.

INTRODUCTION

This report covers the technical progress accomplished under Modification Number 6 to Contract NAS 8-2696 during the period of January 1, 1965 to March 31, 1965.

The report is divided into the following three main sections corresponding to the Part I, II and III Tasks defined in the modified contract.

Part I   Tasks   -   Research and Technology

Part II   Tasks   -   Breadboard and Experimental Items

Part III Tasks   -   System Test Models

For a detailed definition and explanation of these tasks, see the First Quarterly Report, NAS 8-2696-QPR-001, revised January 20, 1965.

PART I TASKS

RESEARCH AND TECHNOLOGY

Fuel Cell Plate Design

A mathematical evaluation of several plate designs was conducted to determine, in particular, their electrical current carrying capabilities. The four different plate designs shown in Figure 1 were considered. The analysis was carried out for the hydrogen plate with the following results:

Design	Millivolt Drop in Hydrogen Plate at 200 ASF	Total Section Drop
1	1.99	5.97
2	2.12	6.36
3	1.26	3.78
4	1.60	4.8

The voltage drop for the oxygen plate is twice the value for a hydrogen plate, since it carries twice the current. Thus the total drop for a section is three times the hydrogen plate drop.

Design 1 is the configuration used in previous Allis-Chalmers modules. Design 2 was not considered because of its higher electrical resistance; design 3 was dropped because of mechanical considerations in assembly. Design 4 is expected to be used in future modules.

The savings in voltage drop between designs 1 and 4 for a single section is 1.17 millivolts at 200 ASF. While in itself this is not a large reduction, a

sizeable saving occurs in the external connections between sections. The voltage drop in the connection under the most favorable conditions has been measured to be 16 to 19 millivolts for a module current of 80 amperes. By introducing a second parallel current lead-off from each cell, the current through each lead-off is cut in half, and consequently, the total voltage drop in the external connections is also cut in half. The 16 to 19 millivolt drop at 80 amperes is roughly the drop expected at 200 ASF for design 1. For design 4, the drop at 200 ASF should be 8 to 9 millivolts.

The voltage savings between designs 1 and 4 are obtained at the expense of approximately 2.4 pounds of added material weight. To get this amount of weight back as a savings in fuel due to improved efficiency, the module would have to be used for a mission requiring a minimum of 247 KWH of energy. For shorter missions design 1 is more economical. For a mission requiring 2000 KWH, design 4 will result in a net savings of 14.4 pounds.

Thermal Analysis Program

"In-Duct" Heaters - The steady state thermal analyzer computer program, previously developed, has been extended into a program capable of handling transient thermal cases. Initial runs of the program for a typical "in-duct" heater arrangement have indicated that substantial temperature gradients may be induced in the module stack during the heat-up period. Operating specifications call for heating up the fuel cell module from 0° F to 190° F in one hour.

The analysis of the "in-duct" heater arrangement studied was based upon the

following considerations:

(1)   Duct and heater parameters

Perimeter	P_d	Density	ρ
Thickness	t_d	Specific heat	C_d
Length increment	dz	Heat flux	H_d $\left(\dfrac{Heat}{Area}\right)$
Total length	L_d	Temperature	T_d

(2)   Coolant parameters

Flow at any point z $\dot{W}(z) \ = \ 2\,\dot{W}g\,(L_d - z)$

Specific heat C_{pg}

Heat transfer coefficient h

Temperature of gas T_e

Heat Balance on duct

      Heat in - Heat out = Heat stored

$$H_d\,P_d\,dz \ - \ h\,P_d\,dz\,(T_d - T_e) \ = \ \rho\,t_d\,P_d\,dz\,C_d\,\frac{d\,T_d}{d\,\theta}$$

Heat Balance on coolant

      Heat in = Heat transported

$$h\,P_d\,dz\,(T_d - T_e) \ = \ 2\,\dot{W}g\,(L_d - z)\,d\,T_e$$

Simplifying the two equations leads to

(1)
$$\frac{d\,t_d}{d\theta} = \frac{h}{t_d\,C_d}\left[\frac{H_d}{h} - (T_d - T_e)\right]$$

(2)
$$\frac{h\,P_d}{2\,\dot{W}\,g}\left(\frac{dz}{L_d - z}\right) = \frac{d\,T_e}{T_d - T_e}$$

The equations are coupled. No exact solution has yet been found. If T_e in the equation is assumed to be independent of time, and T_d in the second equation is assumed to be independent of position, then both equations are integrable. The solutions are:

1.1
$$T_d = \frac{H_d}{h} + T_e - \left[\frac{H_d}{h} - (T_{do} - T_e)\right]\exp\left(\frac{h\,\theta}{t_d\,D_d}\right)$$

2.1
$$T_e = T_d - \left(T_d - T_{eo}\right)\left(1 - \frac{z}{L_d}\right)^{\left(\frac{h\,P_d}{2\,\dot{W}\,g}\right)}$$

The value of T_e is required at the entrance of each cell channel. The program calculates these for each channel (a particular z) and also calculates a duct temperature at this z based on the gas temperature. At the time $\theta = 0$ all T_d's are equal to the initial value T_{do} . An initial value of $T_e = T_{eo}$ is known and T_e's are calculated. Using these T_e's a new set of T_d's are calculated. These will be used in the next set of calculations for T_e . An

example is given in Table I. From this it can be observed that T_e does vary with time, however, the variation is slow when compared with T_d. Also T_d varies with position, but slowly compared with T_e. Thus the assumption on T_d and T_e are approximately true.

Safety and material considerations require that the maximum temperature within the module be held below some limit. For a fiberglass resin duct material, a limit of 250° F is probable. Since a typical value of

$$\frac{H_d}{h} \text{ is } 400° F, \quad \text{and} \quad \frac{h}{\rho \, t_d \, C_p} \text{ is near } 10 \text{ per hour,}$$

the limit of 250° F will be exceeded very rapidly. The hottest point will be at the maximum z . At this point the flow of coolant is the lowest; thus cooling of the duct will be slow when the heaters are turned off.

The use of a duct material such as aluminum may allow a maximum temperature near 400° F (or greater). The higher thermal conductivity of such a material would allow more rapid cooling during a heater cooldown period.

A temperature gradient within the stack will be induced during warm-up. This is due to the rapid variation of T_e along the stack. The speed with which conduction through the stack can eliminate this gradient has not yet been accurately determined.

Results of an initial run are presented in Figure 2. The maximum temperature assumed by the duct has not been shown. It was initially 0° F and is limited to the range of 245 to 250° F. For this case the heater extended over only 60% of the length of the duct. This was done to aid in the cooling of the duct. Input data required to produce this figure are shown on Table II.

For the case presented in Figure 2, the 16th cell temperature would have been 170° F after one hour. The temperature gradient within the stack would have been nearly 50° F.

Future work on this problem will be directed toward estimating the rate at which heat can be transported along the axis of the stack. The effect of using an aluminum duct and a maximum temperature of 400° F will also be considered.

Water Recovery and Purity

Water Recovery Methods - The Hilsch vortex tube is a simple device which splits an inlet gas stream into two lower pressure streams one of which has a temperature higher than the inlet stream, the other a lower temperature. Theoretically a portion of the water vapor leaving a fuel cell would condense in such a device without the need of a heat sink. The heat of condensation would be rejected as sensible heat in the high temperature stream.

An analysis was performed to determine the maximum percentage of the generated steam (from the fuel cell) that could be condensed by a Hilsch tube, assuming an ideal reversible process. The calculations showed that only 1.75% of the steam could be condensed when the hot stream outlet was at 160° C. The amount was so small that the investigation was dropped.

Design of a Water Recovery Device - An analysis of a water recovery device consisting of a condenser and a capillary membrane separator has been completed. A schematic drawing of the condenser-separator unit is shown in Figure 3. This unit accepts water vapor from the Moisture Removal Subsystem of the fuel cell. The water vapor is condensed, passed through the separator and finally transported to an accumulator. Vehicle coolant is used to cool the condensing surface. The water leaving the unit must be sub-cooled to 110° F so that subsequent operations in the Water Recovery Subsystem, which result in lower pressure, will not cause the water to flash into steam.

The case of a 2 KW fuel cell system generating water vapor at a pressure of 5 psia and 195° F was analyzed. Water-methanol (60% methanol and 40% water by weight) was selected as the coolant. The flow rate and temperature rise were assumed to be 100 pounds per hour and 40° F respectively. It was also assumed that the water vapor would be condensed and subcooled to 110° F. Figures 4 and 5 present the approximate area of heat transfer plate and pressure drop in the coolant for rectangular grooves of various sizes.

For the case considered, it was found that the rectangular groove design would cause a smaller pressure drop in the coolant than the design with circular sector shaped grooves. Also, the larger the number of grooves, the smaller will be the required area of the heat transfer plate.

Water Acceptability Monitor - A survey has been made of methods applicable to the inflight monitoring of the quantity of KOH transported from the fuel cell system to the water recovery subsystem. Consideration was limited to those methods which utilize the change in physical properties of the water with changing KOH content. No consideration was given possible systems requiring chemical sample analysis or addition of materials to the water.

Four methods which offer promise for inflight use are pH measurement, conductivity measurement, osmotic pressure measurement, and interferometric determination of changes in refractive index. Only the pH and conductivity methods are useful at KOH concentration levels corresponging to pH 10 or below.

The pH method offers the advantage of instantaneous response, specificity for the hydroxyl ion, and uniform sensitivity for all concentrations of KOH up to the one molar level. The disadvantages for inflight use are serious in that the reference electrode is vulnerable to drying if exposed to cavity vacuum. Also, a continuous flow of KCl from a reservoir to the reference electrode is required for operation of the unit.

The conductivity method offers the advantages of sensitivity over the relevant concentration range, instantaneous response, simplicity, and reliability. The principle disadvantage is non-specificity. Relatively small quantities of ionic impurities in the product water would give spurious indications of high KOH content. However, both pH and conductivity will be given further consideration for application to inflight monitoring of the KOH content of the product water.

Cell Performance Characteristics

Four of the two-cell modules in the continuing test series designed to determine effects of operating and construction parameters are presently on test.

Two of the test cell modules are being used to determine the properties of cells constructed with Allis-Chalmers HYSAC #8 cathodes and with 0.020" thick electrolyte membranes. Preliminary data collected after the first 210 hours of operation at a current density of 200 ASF and a temperature of 190° F was analyzed as follows. A straight line was fitted to the voltage versus time data by means of a least squares method. The zero-time voltage value and the rate of degradation given by the regression lines are presented in the following tabulation:

	HYSAC Cathode	
	Type A	Type B
Current density, ASF	200	200
Time under load, hours	632	498
Potential at zero time, mv	893	888
Degradation rate, microvolts/hour	35.0	66.3

The other two test cell modules are being used to determine concentration and volume of electrolyte required for optimum performance. To date, these cells have logged 1,153 and 184 hours of operation.

Advanced Control Techniques

Determination of Mode of Control of Fuel Cell Temperatures - The computer program now contains an option for the method of temperature control at normal operating temperatures. The two choices are: a proportional type of control, or a semiderivative type of control. The semiderivative control is similar to that now used on breadboard modules and scheduled for use on centerline modules. Figure 6 shows a small segment of the output of a run using the semiderivative type control. Table II shows the major input items required to produce this output.

A mathematical model for the control of fuel cell temperature has been constructed. Various modes of control were investigated and the most applicable of these were analyzed on a computer. The results of this study are presented in graphical form and a comparison is made among widely differing values of control sensitivity.

The control of fuel cell temperature will be accomplished by the regulation of the primary coolant flow rate. The heat extracted by the heat exchanger is a function of the flow rate, inlet temperature, density, and specific heat of the primary coolant and the thermal characteristics of the heat exchanger, in addition to physical properties of the secondary coolant. The mathematical model of this heat transfer process was considered to be a temperature reservoir in thermal contact with the secondary coolant gas. It was found that the mode in which the temperature of the reservoir must be varied by insure a stable fuel cell temperature was the same as the required mode of variation of the primary coolant flow rate.

This relationship can be presented in the following form
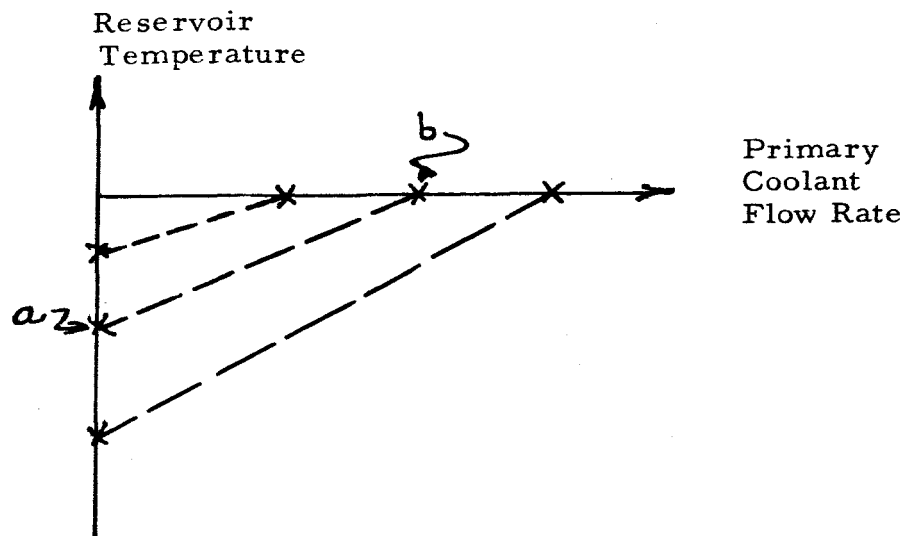
where the points at opposite ends of the dashed lines have equal effects. That is, point a, according to the mathematical model, will extract a certain quantity of heat under certain operating conditions; while point b, the primary coolant flow rate of an actual module, will extract the same quantity of heat under the operating conditions assumed in the calculation of point a. Hence, the mathematical manipulation of the reservoir temperature corresponds to a physical manipulation of the flow rate.

In terms of this reservoir temperature, a system configuration of the form shown below was constructed.
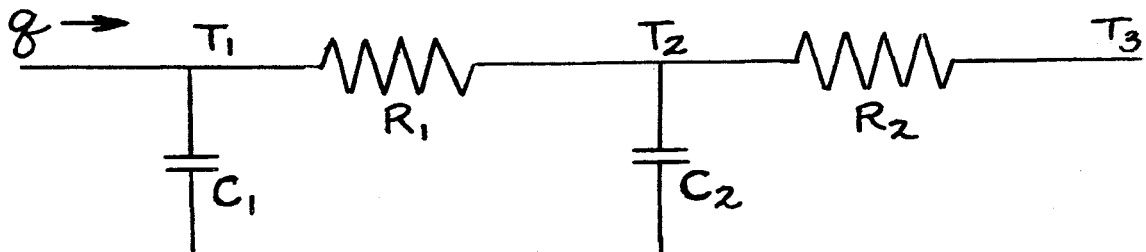
where

q = heat input

T_1 = temperature of fuel cell stack

C_1 = heat capacity of fuel cell stack

R_1 = thermal resistance between fuel cell stack and secondary coolant

T_2 = temperature of secondary coolant

C_2 = heat capacity of secondary coolant

R_2 = thermal resistance of heat exchanger

T_3 = reservoir temperature.

In the above system configuration the following assumptions and approximations were made:

(1) q includes: heat generated by electrochemical reaction, and heat out by water removal.

(2) T_1 and T_2 are spacially homogeneous.

(3) Radiation effects are negligible.

(4) Heat capacity of canister shell, ducts, supply tubing, etc., have been omitted.

An analysis of this configuration yields the following results:

$$T_1 = A T_3 + B q \qquad (1)$$

where

$$A = 1/a\ s^2 + b\ s + 1$$

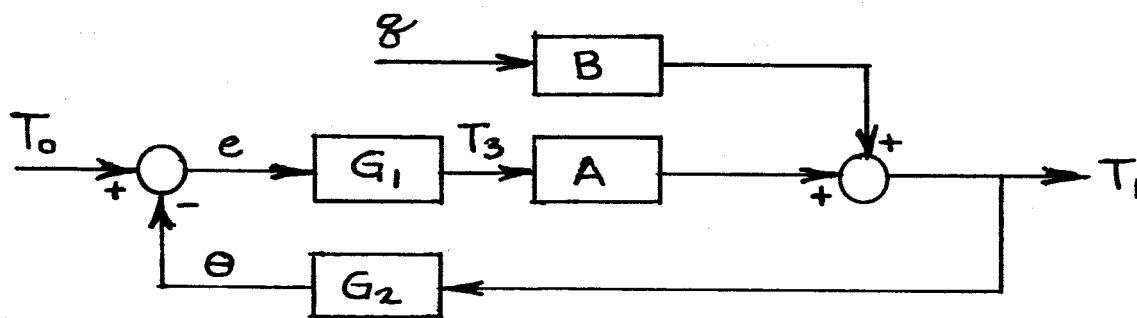$$B = c\ s + f/a\ s^2 + b\ s + 1$$

$$s = \text{time derivative}$$

where:

$$a = R_1 C_1 R_2 C_2$$

$$b = R_1 C_1 + R_2 C_1 + R_2 C_2$$

$$c = R_1 C_2 R_2$$

$$f = R_1 + R_2$$

If a control system to manipulate T_3, and a dead time function, are included, the following system block diagram can be evolved,

where

$$T_o = \text{set point temperature}$$

$$e = T_o - \Theta = \text{deviation}$$

$$G_1 = \text{control function}$$

$$G_2 = \text{dead time function}$$

$$T_3 = \text{manipulated variable}$$

$$\Theta = \text{feedback temperature}$$

-13-

There are three basic types of continuous control action. They are:

(1)   Proportional Control - There is a continuous linear relation between values of the deviation and the manipulated variable.

(2)   Integral Control - The value of the manipulated variable is changed at a rate proportional to the deviation.

(3)   Derivative Control - The value of the manipulated variable is proportional to the rate of change of the deviation.

Automatic control may be achieved by various combinations of the above three modes. The characteristics of this temperature system (i.e., a number of thermal storage elements and dead time) indicate that the proportional-derivative combination is the simplest one that will provide adequate regulation of fuel cell temperature.

For proportional-derivative control,

$$G_1 = K_c (1 + T_d s) \qquad (2)$$

where:

$$K_c = \text{proportional sensitivity}$$
$$T_d = \text{derivative time}$$

The dead time function is,

$$G_2 = \epsilon^{-Ls} = \frac{2 - Ls}{2 + Ls} \qquad (3)$$

where:

$$T_a = \frac{c}{f} \quad , \quad T_b = \sqrt{\frac{a}{1 + K_c}}$$

$$S = \sqrt{\frac{(b + K_c T_d)^2}{4 a (1 + K_c)}}$$

Or, in differential form:

$$T_b^2 \ddot{e} + 2 S T_b \dot{e} + e = \left[\frac{f}{1 + K_c}\right] (T_a \dot{q} + q)$$

For a step change in $q = Q$,

$$T_b^2 \ddot{e} + 2 S T_b \dot{e} + e = E_o = \left[\frac{f}{1 + K_c}\right] Q = \text{Offset}$$

From previous experimental data approximate numerical values have been obtained for the following constants:

$$R_1 = 2 \times 10^{-3} \text{ hour } {}^\circ\text{F / BTU}$$

$$C_1 = 20 \text{ BTU / }{}^\circ\text{F}$$

$$R_2 = 2 \times 10^{-2} \text{ hour } {}^\circ\text{F / BTU}$$

$$C_2 = 8 \times 10^{-3} \text{ BTU / }{}^\circ\text{F}$$

where:

ϵ = base of natural logrithims

L = dead time

For a constant value of set point temperature, the deviation as a function of heat can be determined as shown below.

$$e = \left[\frac{X}{Y} \right] q \qquad (4)$$

where:

X = $g s^2 + h s + k$

Y = $m s^3 + n s^2 + p s + r$

and g = $L c$

h = $2 c + L f$

k = $2 f$

m = $a L$

n = $2 a + b L - K_c T_d L$

p = $2 b + L - K_c L + 2 K_c T_d$

r = $2 + 2 K_c$

If the time lag (dead time) be zero, the equation reduces to:

$$e = \left[\frac{f}{1 + K_c} \right] \left[\frac{T_a s + 1}{T_b^2 s^2 + 2 S T_b s + 1} \right] q$$

where:

$$T_a = \frac{c}{f} \quad , \quad T_b = \sqrt{\frac{a}{1 + K_c}}$$

$$S = \sqrt{\frac{(b + K_c T_d)^2}{4 a (1 + K_c)}}$$

Or, in differential form:

$$T_b^2 \ddot{e} + 2 S T_b \dot{e} + e = \left[\frac{f}{1 + K_c} \right] (T_a \dot{q} + q)$$

For a step change in $q = Q$,

$$T_b^2 \ddot{e} + 2 S T_b \dot{e} + e = E_o = \left[\frac{f}{1 + K_c} \right] Q = \text{Offset}$$

From previous experimental data approximate numerical values have been obtained for the following constants:

$$R_1 = 2 \times 10^{-3} \text{ hour } °F / BTU$$

$$C_1 = 20 \text{ BTU} / °F$$

$$R_2 = 2 \times 10^{-2} \text{ hour } °F / BTU$$

$$C_2 = 8 \times 10^{-3} \text{ BTU} / °F$$

A step change in heat input due to a sudden increase in the output power of the cell produces the following effects:

Let Q = 2000 BTU/hour

With K_c = 0 (i.e., without any control); E_o = 44° F

But with K_c = 200;

$$E_o = 0.2° F$$

However, if K_c be considered as large as 200, then S = 0.6 and the temperature response of the fuel cell becomes underdamped.

$S > 1$, overdamped

$S = 1$, critically damped

$S < 1$, underdamped

If is only then (when $S < 1$), that derivative control becomes useful in suppressing the oscillations.

It is estimated that the dead time, L, in the system is less than 15 seconds. In order to obtain the response of the control system with the time lags included, the functional relationships of the system block diagram were reconstructed for analysis on an analog computer. However, a digital computer program which simulates the operation of an analog computer has previously been set up. This is the program that was used in these determinations.

The computer analysis demonstrated the effect of the control system as a function of heat input. The system was subjected to a heat input step function with no control, and then the process was repeated a number of times under differing amounts of control sensitivity.

Figures 7 through 11 are a graphical representation of the computer results. The following notations are made for these graphical representations:

Figure 7 - The period of the heat input function consists of four 45 minute intervals. The time axis of the graphs are sectioned in 45 minute intervals where section a corresponds to zero heat input, b to 1000 BTU/hour, c to 4000 BTU/hour, and d to zero BTU/hour.

Figure 8 - Both the value of the offset temperature, and the time required to reach offset is considerably decreased when proportional control is introduced.

Figure 9 - When the proportional sensitivity is made large, K_c = 100, the fuel cell temperature begins to show signs of instability but eventually settles down to a steady offset value. At K_c = 200, instability has completely set in and the temperature continues its oscillations indefinitely.

Figure 10 - With K_c = 200, non-stable condition exists. The introduction of derivative control suppresses the oscillations and allows the fuel cell temperature to return to a steady value. The final offset value is lowered by increasing the derivative time, T_d.

Figure 11 - With K_c = 100, and T_d = 0; the fuel cell temperature, heat input, and value of control variable, (reservoir temperature or alternatively, primary coolant flow rate), are plotted on the same time axis to show the time relationship among them. The existance of the time lag, L, is the direct cause for the appearance of the oscillations.

From the above results it can be concluded that a proportional-derivative control system will maintain the temperature of the fuel cell within any reasonable limits without any inherent instability, provided a proper choice is made for the values of proportional sensitivity and derivative time.

Reactant Gas Pressure Surges in a Fuel Cell - The reactant gases are supplied to the fuel cell plates through a few feet of tubing. If the direct current developed by a fuel cell is converted to alternating current, there would be a periodic demand on the fuel cell causing periodic gas consumption. The inertia of the flowing gas in the tubing coupled with the gas capacitance of the tubing may then induce excessive pressure surges. Sample calculations have been made with a computer to specify the order of magnitude of this effect, since such a resonant condition might cause undesired mechanical vibration. The frequency and gain of this resonant condition have been determined in the following manner.

A model for the reactant gas subsystem was adopted as shown in Figure 12. The electrical analog for the system in Figure 12 was determined to be:

where

$$Z_1 = R_1 + jwL$$

-19-

$$Z_2 = \frac{1}{j w C_1}$$
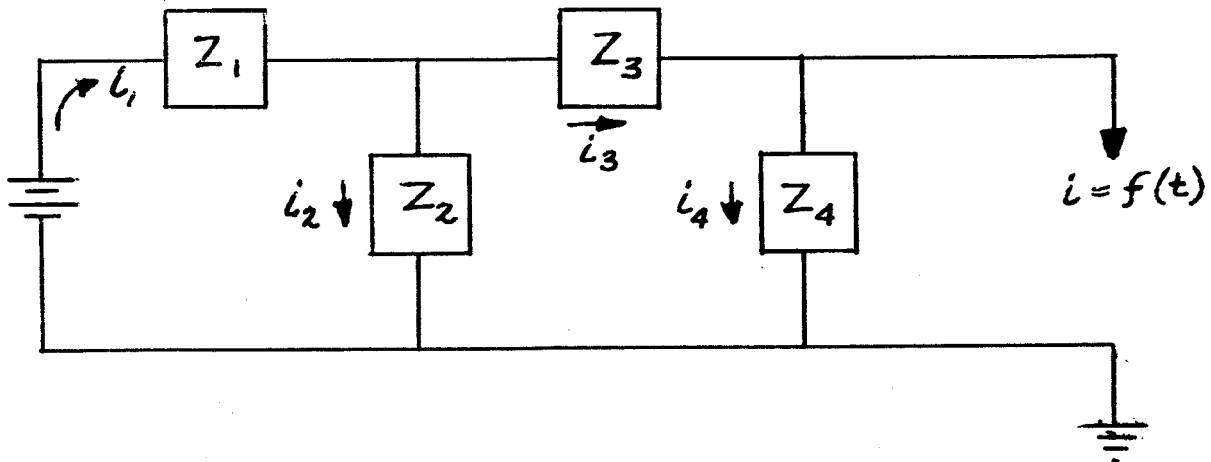
$$Z_3 = R_2$$

$$Z_4 = \frac{1}{j w C_2}$$

E = constant "voltage" (35 psia)

e_1 = manifold and inlet tube "voltage" (pressure)

e_2 = plate "voltage" (pressure)

i = "current" outflow as a function of time (consumption rate)

The defining relations were:

(i) $\quad E - e_1 = Z_1 i_1$

(ii) $\quad e_1 - e_2 = Z_3 i_3$

(iii) $\quad e_1 = Z_2 i_2$

(iv) $\quad e_2 = Z_4 i_4$

(v) $\quad i_1 = i_2 + i_3$

(vi) $\quad i_3 = i_4 + i$

Eliminating i_1, i_2, i_3, i_4, and e_2 from the six equations yielded the following equations:

$$Z_5 e_1 = Z_6 E - Z_7 i$$

where:

$$Z_5 = Z_2 Z_3 + Z_1 Z_3 + Z_1 Z_2 + Z_4 Z_2 + Z_4 Z_1$$

$$Z_6 = Z_2 Z_3 + Z_2 Z_4$$

$$Z_7 = Z_1 Z_2 Z_4$$

If $E = E_o = $ constant; then e_1 as a function of i will become,

$$e_1 = - \frac{Z_7}{Z_5} i = - \frac{Z_7}{Z_5} f \quad (t)$$
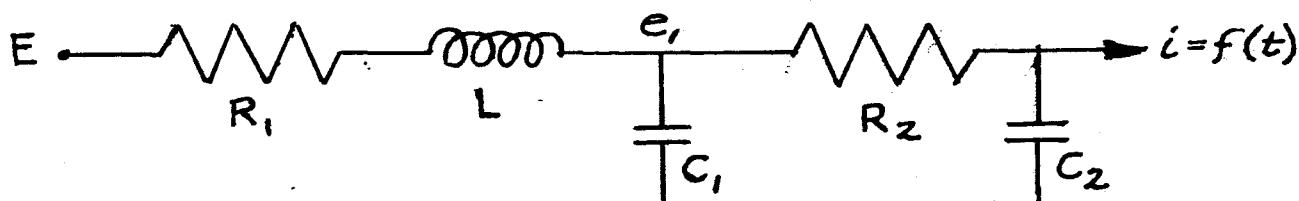
In terms of the original parameters this becomes,

$$e_1 = - Z f (t)$$

where:

$$Z = \frac{L s + R_1}{(R_2 C_2 L C_1) s^3 + (R_1 C_1 R_2 C_2 + L C_2 + L C_1) s^2 (R_2 C_2 R_1 C_2 + R_1 C_1) s + 1}$$

and $s = jw$

From the preceding assumptions and calculations, the following working model
was developed.

-21-

$$E \;—\!\bigwedge\!\bigwedge\!\bigwedge\!—\!\mathrm{L}\;(\text{inductor})—\; e_1 \;—\!\bigwedge\!\bigwedge\!\bigwedge\!— \; i = f(t)$$

E R_1 L e_1 R_2 C_1 C_2 $i = f(t)$

The numerical values of the constants in the above model for both the oxygen and hydrogen systems are enumerated below. The asterisked quantities are those used in evaluating Z.

		OXYGEN	HYDROGEN	UNITS
Flow rate (I = 70 amps)	w	4.45×10^{-4}	5.5×10^{-5}	lbs/sec
Viscosity (32° F)	μ	1.27×10^{-5}	5.6×10^{-6}	lbs/ft sec
(195° F)	μ	1.59×10^{-5}	6.7×10^{-6}	lbs/ft sec
Density (32° F, 14.7 psia)	ρ	8.92×10^{-2}	5.6×10^{-3}	lb/ft³
(32° F, 35 psia)	ρ	2.12×10^{-1}	1.33×10^{-2}	lb/ft³
(195° F, 35 psia)	ρ	1.59×10^{-1}	1.01×10^{-2}	lb/ft³
Inlet Tubing (32° F, 35 psia)	1			
Length	ℓ_1	2	2	ft
Diameter	d_1	3.1×10^{-2}	3.1×10^{-2}	ft
Capacity	C_{ℓ_1}	9.2×10^{-6}	5.8×10^{-7}	in²
Resistance	R_{ℓ_1}	1.14	8.0	sec/in²
Flow rate (I = 70 amps)	w_1	2.1×10^{-3}	4.1×10^{-3}	ft³/sec
Flow velocity (I = 70 amps)	v_1	2.78	5.5	ft/sec
Reynolds Number	N_{Re_1}	1440	400	------

		OXYGEN	HYDROGEN	UNITS
Manifold (195° F; 35 psia)	2			
Length	ℓ_2	2	2	ft
Diameter	d_2	3.1×10^{-2}	3.1×10^{-2}	ft
Capacity	C_{ℓ_2}	6.9×10^{-6}	4.3×10^{-7}	in^2
Resistance	R_{ℓ_2}	1.90	12.6	sec/in^2
Flow rate (I = 70 amps)	w_2	2.8×10^{-3}	5.5×10^{-3}	ft^3/sec
Flow velocity (I = 70 amps)	v_2	3.7	7.24	ft/sec
Reynolds Number	N_{Re_2}	1150	340	-----
Cell Plates (195° F, 35 psia)	③			
Volume (35, 70 plates)	V	2.6×10^{-2}	5.2×10^{-2}	ft^3
* Capacitance (35, 70 plates)	C_2	1.19×10^{-4}	1.49×10^{-5}	in^2
Slot (195° F, 35 psia)	④			
Length (each)	ℓ_3	5.2×10^{-2}	5.2×10^{-2}	ft
Height (each)	z_1	3.3×10^{-3}	3.3×10^{-3}	ft
Width (each)	z_2	2.1×10^{-2}	2.1×10^{-2}	ft
Aspect ratio function	α	0.05	0.05	---
Flow rate (each)	w_3	8.0×10^{-5}	7.9×10^{-5}	ft^3/sec
Flow rate (35, 70)	w_4	2.8×10^{-3}	5.5×10^{-3}	ft^3/sec
Reynolds Number	N_{Re_3}	100	15	---
Resistance (each)	R_a	18.7	126	sec/in^2
* Resistance (35, 70)	R_2	0.54	1.8	sec/in^2
Supply Volume	①&②			
* Resistance	R_1	2.09	14.3	sec/in^2
Length	ℓ	3	3	ft
Density	ρ	1.94×10^{-1}	1.22×10^{-2}	lb/ft^3
* Inertial Inductance	L	0.89	0.80	sec^2/in^2
* Capacitance	C_1	1.61×10^{-5}	1.01×10^{-6}	in^2

If $R_2 = 0$, a simple series L-C-R circuit is left, whose natural frequency is

$$f = \frac{1}{2\pi} \left[\frac{1}{LC} - \frac{R^2}{4L^2} \right]^{\frac{1}{2}}$$

where

$$R = R_1$$

$$C = C_1 + C_2$$

The resonant frequency of this circuit occurs when,

$$f = \frac{1}{2\pi \sqrt{LC}}$$

The centerline values of the fuel cell yield $\frac{1}{LC} \gg \frac{R^2}{4L^2}$, therefore, the natural frequency and the resonant frequency, f_o, are approximately equal.

Numerically: $\qquad f_o = \begin{cases} 14.5 \text{ Hz for oxygen} \\ 27.0 \text{ Hz for hydrogen} \end{cases}$

At the other extreme, if $C_2 = 0$, the resonant frequency becomes

$$f_o = \begin{cases} 43 \text{ Hz for oxygen} \\ 150 \text{ Hz for hydrogen} \end{cases}$$

The resonant frequency of the actual system should lie between the two extremes calculated above.

The complete system (for oxygen) has been analyzed on a computer, giving:

Resonant frequency, f_o = 14.6 Hz

Gain at f_o = 2600

The gas consumption is of the form $i = i_{max} \sin wt$. For maximum consumption (current = 70 amperes) $i_{max} = 4.6 \times 10^{-5}$ pounds of oxygen per second which corresponds to a maximum overpressure of 0.12 psia. A graphical plot of these results are presented in Figure 13.
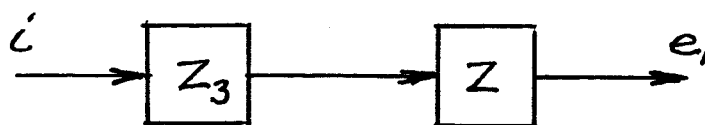
A further refinement was made by considering the resistive and capacitive effects of the reactant gas that is dissolved in the electrolyte located within the electrodes.

Dissolved Gas		OXYGEN	HYDROGEN	UNITS
Capacitance	C_3	8.8×10^{-8}	4.5×10^{-8}	in^2
Resistance	R_3	4.8×10^{5}	3.8×10^{6}	sec/in^2

The resulting system is now:
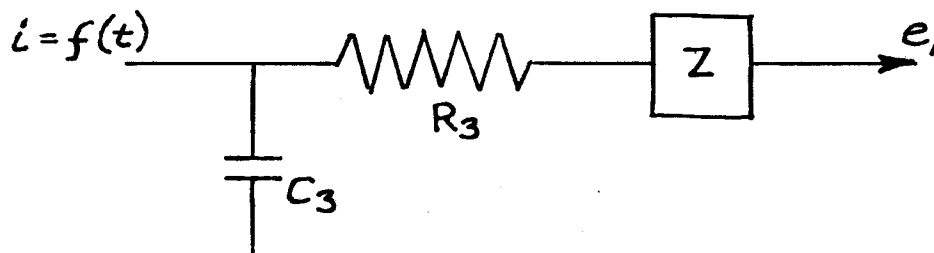
or

where:

$$Z_3 = \frac{1}{R_3 C_3 s + 1}$$

Adding this R-C leg onto the previous configuration yields:

Resonant frequency,
gain at f_o = 700   =   14.6 Hz

Maximum consumption would produce a maximum overpressure of 0.031 psia. A graphical plot of these results is also presented in Figure 13.

PART II TASKS

BREADBOARD AND EXPERIMENTAL ITEMS

Allis-Chalmers Breadboard Number 1 (A-C BB # 1)

At the successful conclusion of a load performance test of 404 hours, A-C BB # 1 was used in conducting a series of non-operating tests to determine the resistance of the secondary coolant flow path. (For a report of the 404 hours performance test see NAS 8-2696-QPR-002, the Second Quarterly Progress Report.) This 404 hour test established the August 1964 base technology of the Allis-Chalmers fuel cell system. Since this time a number of advanced systems have been built, or are in the process of being built. Any further testing of this unit built to this early technology would produce results of only limited value. With advanced units available for test, it was decided to discontinue performance testing of A-C BB # 1.

MSC 1.8 KW Breadboard

Upon completion of 500 hours of testing under load, which exceed the contractual goal of 200 hours by 2.5 times, the unit still was in excellent operating condition. The unit was stored for two months and testing was then resumed.

At the end of this reporting period over 700 hours of operation under load have been logged by this unit, and at the average load of approximately 1000 watts, the output voltage was still within 95% of its original value. Figure 15 (A) shows the volt-power performance characteristics through 605 hours of operation. Testing of the unit at MSC will continue until its useful life is expended, or until 1000 hours of operating time is reached, whichever occurs first.

Allis-Chalmers Breadboard Number 2 (A-C BB # 2)

The construction of A-C BB # 2 was completed and this fuel cell system was placed on test on January 22, 1965. A major test objective of this 2 KW system is an endurance test run of 1000 hours after which the accumulated test data will be thoroughly analyzed.

The significant technological advancements in the design of A-C BB # 2, notably an improved silver cathode, resulted in power growth and improved efficiency in addition to improved electrical performance. The number of cells was reduced from 70 to 62, the weight of the canister assembly was correspondingly reduced 12 percent under the MSC unit, and the volume of the canister was decreased by 11 percent. The average cell efficiency of A-C BB # 2 was 78 percent compared to 73 percent for the MSC unit; at 1800 watts the cell efficiency was 74 percent compared to 66 percent. The fuel cell module with canister removed, is shown in Figure 14.

Figure 15 (B) shows the volt-power performance characteristics of A-C BB #2 through the 720 hours of operation that have been logged to date. Comparisons of the MSC and A-C BB # 2 performance characteristics show a definite improvement in voltage regulation, total power and life, as indicated by the flatness of the V-P curves. At 430 hours the voltage at 1000 watts output of both units was 98 percent of its initial value, but at 1800 watts A-C BB # 2 was capable of 94.5 percent of its initial voltage; whereas, the MSC unit produced 85.8 percent of initial voltage. During 720 hours of operation A-C BB # 2 produced 836 KWH of energy compared to 673 KWH of energy produced by the MSC unit during 700 hours of operation.

All performance tests were run using commerical grade reactants, which adversely influenced the purge requirements and degradation characteristics. Results nevertheless were favorable. Purging required about 3.6 percent of the stoichiometric fuel. Tests with ultra-pure gas are underway at MSC and indicate a considerably reduced purge requirement.

Some variations in individual cell section voltages were noted during operation of the MSC unit. These variations are related in part to the dimensional tolerance variations allowed for the cell components. Cell section voltage variations have been reduced on A-C BB #2 by more stringent cell component tolerances.

PART III TASKS

SYSTEM TEST MODELS

Fabrication of System Test Models

The design specifications for the first four of the eight advanced 29 volt, 2000 watt fuel cell power systems to be built has been completed, and fabrication of the first two units (Systems No. 5 and 2) is in progress. The fuel cell module for System No. 5 has been assembled, and the various subsystem assemblies are being built. Fabrication of long lead time items for the second two units (Systems No. 3 and 4) also is in progress. Purchase orders for all vendor-furnished components have been issued and design verification testing of these components is being initiated as the components are received. The following components are now on test:

(a)   Pressure Regulators

(b)   Water Removal Solenoid Valve

(c)   Pressure Transducers

(d)   RPM Sensor

(e)   Reactant Inlet Solenoid Valve

(f)   Cooling Blowers

The following Engineering and Development Tests were conducted during this reporting period.

Fuel Cell Assembly Vibration Tests

Vibration testing was conducted on an equivalent vibration model of the cell

assembly at NASA - Huntsville from March 15 through March 18 with Allis-Chalmers personnel present to view the testing.

The vibration program imposed was as follows:

(1)   Sinusoidal Sweep Test - perform a log sine sweep test from 5 to 2000 cps and from 2000 to 5 cps at the following input level at the rate of one octave per minute in three mutually perpendicular axes.

$$
\begin{array}{llll}
5 - 28 & cps & - & 0.75 \text{ in. D.A.} \\
28 - 115 & cps & - & 3.0 \text{ G peak} \\
115 - 240 & cps & - & 0.0024 \text{ in. D.A.} \\
240 - 2000 & cps & - & 7.0 \text{ G peak}
\end{array}
$$

(2)   Random Test - perform 5 minute random vibration tests in three mutually perpendicular axes at the following input levels:

$$
\begin{array}{llll}
20 - 200 & cps \text{ at} & 9.0 \text{ db/octave} \\
200 - 700 & cps \text{ at} & 0.22 \text{ } g^2/cps \\
700 - 900 & cps \text{ at} & - 18.0 \text{ db/octave} \\
900 - 2000 & cps \text{ at} & 0.05 \text{ } g^2/cps
\end{array}
$$

The axis of vibration and accelerometer locations were as shown in Figure 16.

Results of Test - from the preliminary test data and observations made during testing, the following results were noted:

(1)   No failures occurred.

(2)   No leakage of the fuel cell module or canister occurred.

(3)   The highest recorded vibration level was approximately 30 g's at 100 cps which was measured at accelerometer position # 3 during high level sinusoidal testing in the longitudinal axis. (See Figure 16, Configuration 3, horizontal plane).

Redesigned Fuel Cell Plates

A four-cell test module constructed with redesigned oxygen, hydrogen and water removal plates was performance tested for 240 hours to evaluate the new design. This design includes two electric current take-off tabs and minor modifications to improve the distribution of the reactant gases, and the collection of reactant water. Test results indicated that the performance and moisture removal characteristics of the new design were superior to the previous design. Plates of this new design are being used in the fuel cell modules of the systems being built under Part III Tasks.

Secondary Coolant System Flow Resistance Tests

A thermal mock-up of the fuel cell module and canister assembly was constructed to study the secondary coolant loop flow resistance of the design to be employed for the Part III systems.

Tests were conducted to determine the flow resistance of the secondary cooling loop of the mockup in comparison to A-C BB # 1 and to determine the effect upon the flow resistance of minor variations in the physical configuration of the cooling loop.

Figures 17 through 19 show the results of this testing using air, and calculated for helium and hydrogen as the cooling medium. A reduction in flow resistance (ΔP) of approximately 0.30" H_2O at 55 cfm of helium was accomplished in the thermal mockup in comparison to A-C BB # 1. A further reduction of 0.06" H_2O in ΔP was accomplished by the addition of a slot common to all fins at the entrance of the secondary coolant. Varying the distance between the heat exchanger and the top of the fuel cell module produced no significant changes in the flow resistance. However, it was determined that this distance should not be less than 1.5 inches.

Cooling Blower Life Tests

Two Globe fans, part number 19A751, and one Globe fan, part number 19A921, are presently on life test. Approximately 300 hours of operation have been completed to date; no defects or malfunctioning have been noted.

Moisture Removal and Water Recovery Subsystems

A water recovery subsystem design has been evolved and a breadboard model of the system is under test to verify the design. Results tentatively indicate that the design concept for condensing surface and retaining the liquid water is adequate but the present design does not provide for adequate subcooling of the liquid since a fraction of it is flashing back into the vapor state. In addition, the membrane transport area must be increased by approximately a factor of four to adequately handle the water produced in the system. A modified condenser is being designed with four times the membrane transport area, and with provisions for subcooling the condensate. This condenser will be incorporated into the Water Recovery Subsystems for Systems No. 2 and No. 4.

Condenser Test -

After initial tests of the condenser, it was evident that the amount of condensate that could pass through the membrane was greatly restricted. Inspection of the disassembled condenser showed that the membrane support plaques were too thick. They had been compressed by the end plates during assembly and the membrane pores were closed, stopping the flow of water. When they were replaced by support plaques of proper thickness water passed through the membrane and the condenser functioned properly.

Three modifications of the condenser were tested. These arrangements were:

Modification 1 - Support plaques were replaced with two layers of stainless steel wire cloth.

Modification 2 - The thickness of the membrane was changed from 0.030" to 0.020" and a stainless steel wire cloth support was used. The magnesium water removal end plate was replaced with a plexiglass plate incorporating an increased number of water grooves. Performance tests were not completed because of the rupture of the asbestos membrane during test. A minor rework of the plexiglass plate to eliminate the sharp shearing edge corrected this difficulty.

Modification 3 - Support plaques were used with 0.030" membrane asbestos and the modified plexiglass end plate.

A vent connection to the steam groove in the end plate was provided to allow regulation of the steam pressure in the condenser. Thus during the test when more steam is admitted to the condenser than can be condensed or more condensate formed than can be passed through the membrane, the excess can then be exhausted.

To determine the maximum amount of condensate that could pass through a membrane, tests were conducted which applied liquid water directly into the steam inlet passages of the condenser. Modifications 1 and 2 were tested in this manner and the results are shown on Figure 20. The amount of water passed is a direct function of the pressure differential across the membrane.

Wire cloth asbestos supports are apparently not satisfactory because of erosion of the asbestos by the live steam. Therefore, support plaques were used again

for Modification 3. The erosion effect on the support plaques will be determined after a longer period of testing has been completed.

Figure 21 shows the amount of condensate passing through the membrane versus the total amount of steam entering the condenser (Modification 3). The excess steam was condensed but could not pass through the membrane. This curve indicates the pressure differential across the membrane necessary to drive through a certain amount of condensate.

The coolant pressure drop versus flow rate is shown in Figure 22. The pressure drop values are for the condenser plus a short piece of 3/8" stainless steel tubing in the form of a 90° elbow at both the inlet and outlet connections. The pressure drop is within design limits. The design specification allows for 5 psi maximum at a flow rate of 100 pounds per hour.

Figure 23 is a plot of the coolant temperature rise versus the flow of steam. A theoretical curve has been plotted. The difference in the two curves is probably due to the variation in specific heat of the coolant with temperature and heat transfer to external media.

The results tentatively indicate that:

(1)   The condensing surface is adequate but the design tested does not provide adequate subcooling of the liquid. Visual inspection of the water side of the condenser shows water vapor on the center of the membrane and recondensing as it passes to the cooler end of the condenser. A modification of the cooling design to provide coolant under the condenser membrane will eliminate this problem.

(2)   The membrane area must be increased by approximately four times by stacking four units together, to handle the amount of water being produced by the fuel cell module.

Further tests on the present condenser will be carried out to check the life characteristics of the asbestos and support plaques (Modification 3), and test new support materials which may increase the flow of water.

Electrical Monitoring and Control and Instrumentation Subsystems (EMCS and IS)

The EMCS and IS design specifications were evolved and completed. These specifications are in line with NASA's MSFC recommendations in which all controls are resolved into a system of standard logic elements many of which are available in microminiature form. As a result of this effort, the volume of the electrical controls has been greatly reduced to approximately 500 cubic inches, and can possibly be further reduced in the future by taking advantage of the latest developments in the art of monolithic integrated microcircuits. A packaging arrangement for the controllers has been evolved and is being constructed.

The following is a brief description of the Electrical Monitoring and Control, and Instrumentation Subsystems circuits and their status.

(1)   Temperature Control - The temperature control receives a sustained signal from a thermistor located in the FCA. A transient signal is also received from the shunt of the FCA which senses the magnitude of the total output current. The combined signals control a differential amplifier, and a bi-stable multi-vibrator. The current signal from the shunt is conditioned by a derivative network to provide incipient demand control. The temperature controller will be capable of controlling heat or cooling the FCA.

A published Zero-Crossing Synchronizing Circuit for SCR's has been successfully modified for static control of a 1 KW heater in response

to a signal received from the FCA temperature and coolant controller. Modifications have been designed into the operational amplifier output in the coolant control circuit which permits mating the heater controller with the coolant controller; the entire system being designated as the temperature controller.

A breadboard model of the temperature controller has been built and tested. The output stage of the controller was modified by utilizing uni-junction transistors, thereby increasing reliability. Work has begun to build four prototype models of the controller. The temperature controller will consist of three spearate printed circuits board assemblies; sensing, heating and cooling.

(2)   Purge Controller - The purge controller will schedule purging on an ampere hour basis. The ampere hour element of the unit consists of a conventional uni-junction staircase wave generator with modifications. A straight line relationship between millivolt input from the main current shunt and the pulse frequency is obtained over the range of 1 ampere to 120 amperes. Additional countdown circuitry features a microminiature decade counter driving a switching matrix, which in turn opens the purge valves for a predetermined time interval each time a pulse is received from the switching matrix.

The breadboard model of an ampere-hour related purge valve controller has been demonstrated to be capable of performing scheduled functions on a broad basis (various purge schedules may now be readily set up), strictly related to ampere-hours of fuel cell output, and sequentially interrelated purge valve control with provision for manual override.

Redesign of the purge controller, necessitated by the manufacturer's discontinuation of the microminiature decade counter is in progress.

Changes include an alternate divide by 32 circuit and elimination of the switching matrix. The resulting change has improved circuit stability.

Utilizing conventional pulse feedback techniques it will be possible to set up 32 different purge schedules ranging from a purge once each 1/4 ampere hour to once each 8 ampere hours. It will also be possible to vary each of these schedules using a vernier adjustment located on the staircase network. Without feedback, five different purge schedules ranging from one purge each 1/4 ampere hour to a purge each 8 ampere hours are available and have been verified in the laboratory.

A three input gate has also been incorporated to facilitate an automatic purge input, a Master Control Input, and a Manual Purge Input to the variable seven second maximum delay output stage.

Work has started to build four prototype models of the purge controller. This controller will consist of two printed circuit board assemblies; one containing the sensing and output circuits, and the other, the multiple bi-stable circuit.

(3)   Protective Devices - Utilizing proven concepts, the design of an over-current inverse time relay is progressing satisfactorily. The over-current device will be capable of sensing overload current using the module shunt and removing the load instantaneously for short circuit and in approximately 20 seconds for a 110 ampere load. Figure 24 depicts the proposed current versus trip time goal desired. The theoretical transfer function and laboratory feasibility tests, recently completed, verify the capability of the design to meet the stated requirements. To facilitate more adequate testing, a breadboard model of the circuit is now being constructed.

(4)   Regulated Power Supply - Two independent regulated outputs are required for stable operation of the controllers. The supply will incorporate a switching mode regulator as an integral part of a DC to DC insulating inverter to provide a compact, highly efficient, regulated inverter.

Investigations were conducted on core materials for use as transformers and chokes in the DC to DC inverter. Orthonal and Silectron tape wound cores of various thicknesses as well as torroidol powdered iron cores were studied.

Satisfactory voltage regulation characteristics were obtained. The overall (inverter and voltage regulator) efficiency of the breadboard model presently varies between 65.5 % and 57.1% and is below expectations. The core material used in the inverter and output reactor is presently 12 mil steel which has relatively high losses in this type of operation. The inverter and reactor core will be replaced with 2 mil material which is expected to increase the efficiency.

(5)   Master and Auxiliary Master Control - A breadboard model of this control is in the development stage. Digital logic circuits will be used to simulate all input conditions and the outputs will control lights to simulate valve closing or other outputs.

PROGRAM ANALYSIS

An interpretation of the technical progress of the program to date is presented in this section of the report. The accomplishments and problem areas with respect to the program objectives are analyzed.

PART I - RESEARCH AND TECHNOLOGY

The purpose of the Part I tasks is to advance fuel cell technology and to support the development of the 2 KW fuel cell systems of Part III.

A summary of the effort accomplished under the Part I tasks includes:

(a) An analysis of variation in individual cell performance resulted in definition of critical parameters of cell components. These definitions are being expanded and refined so that upgraded component specifications can be written.

(b) Thermal analysis computer programs to analyze and optimize the fuel cell system thermal design have been evolved. These programs are being expanded and refined as test data becomes available.

(c) An analysis of the present fuel cell system control techniques has been completed. The studies indicate that the controls are adequate for the present power levels.

(d)   Various methods of recovering the fuel cell by-product water have been studied. To date the best approach appears to be the static-condenser and separator concept.

(e)   In conjunction with Item (d) above, methods of determining the acceptability of the recovered fuel cell water prior to its storage is being investigated. The two methods selected for further study are direct pH measurement and ionic conductivity.

(f)   A computer analysis was developed to calculate the voltage loss in the fuel cell support plates. As a result of this analysis the number and location of the electrical pick-up tabs on the plates were modified.

PART II - FUEL CELL BREADBOARD SYSTEMS

The 29 volt, 1.8 KW fuel cell system that was delivered to MSC for NASA evaluation has successfully logged over 700 hours of operation to date, with further testing scheduled.

A 28 volt, 2 KW fuel cell breadboard system was assembled and testing initiated at Allis-Chalmers the latter part of January 1965. To date this system has logged in excess of 720 hours of operation during which it has produced 836 KWH of energy. This system was constructed with improved cathodes and electrolyte vehicles. These improved components have resulted in greatly increased cell efficiency, performance stability, and fuel cell system life.

No serious technological problems have been identified. Efforts to improve the reactant purge design and control methods that will lower the pH of the product water to assure potability are continuing.

PART III - FUEL CELL SYSTEM TEST MODELS

Design specifications have been completed for the first four 2 KW fuel cell systems of Part III (Systems # 5, # 2, # 3 and # 4). Hardware components such as reactant pressure regulators, solenoid valves, pressure transducers, etc., have been purchased and received. Design Verification Testing of these components is in progress.

The first generation of the automatic controls for System # 5 have been assembled and are undergoing checkout tests.

The fabrication of System # 5 is complete and the assembly of the various sub-systems is in progress. The fabrication of Systems # 2, # 3 and # 4 are in progress.

The feasibility testing of the Water Recovery Subsystem has been completed. The WRS design for Systems # 2 and # 4 has been evolved and these subsystems are in fabrication.

To date, the Part III efforts are on schedule and no major problem areas have been encountered.

TABLE I

Sample Calculation for Figure 2

$$T_d = 400 + T_e - \left[400 - (T_{do} - T_e) \right]^{-10\theta}$$

$$T_e = T_d - (T_d - T_{eo}) \left(1 - \frac{Z}{L_d}\right)^2$$

Time in Hours		POSITION			
		0	0.25	0.5	1.0
	T_{do}	0	0	0	0
0	T_{eo}	0			
	T_e	0	0	0	0
	T_d	0	0	0	0
0.01	T_{eo}	0			
	T_e	0	0	0	0
	T_d	38	38	38	38
0.02	T_{eo}	0			
	T_e	0	16.6	29.5	38
	T_d	72	76	78	80
0.03	T_{eo}	0			
	T_e	0	33	58	80
	T_d	104	113	120	125

TABLE II

Major Input Items Required to Produce Figure 2

Number of Sections	32
Secondary Coolant Flowrate per Channel	0.25 pounds per hour
Density of Duct	100 pounds/ft^3
System Heat Capacity	25 BTU/° F
Secondary Coolant Specific Heat	3.47 BTU/pound ° F
Specific Heat of Duct	0.5 BTU/pound ° F
Heat Flux from Heater	2000 BTU/hour ft^2
Maximum - Minimum Duct Temperature	250° F - 245° F
Relative Distance Along Duct of Heater Material	62.5 %

TABLE III

Major Input Items Required to Produce Figure 6

Number of Sections	32
Primary Coolant Flowrate	150 pounds per hour
Secondary Coolant Flow per channel	0.25 pounds per hour
Heat Exchanger Capacity	100 BTU/ ° F
Cell Performance	$V = 1.02 - 0.0007$ (ASF)
Primary Coolant Specific Heat	0.75 BTU/pound ° F
Secondary Coolant Specific Heat	3.47 BTU/pound ° F
System Heat Capacity	25 BTU/ ° F
Primary Coolant Inlet Temperature	50° F
Bypass Valve Closed Period	0.01 hours

DESIGN #2
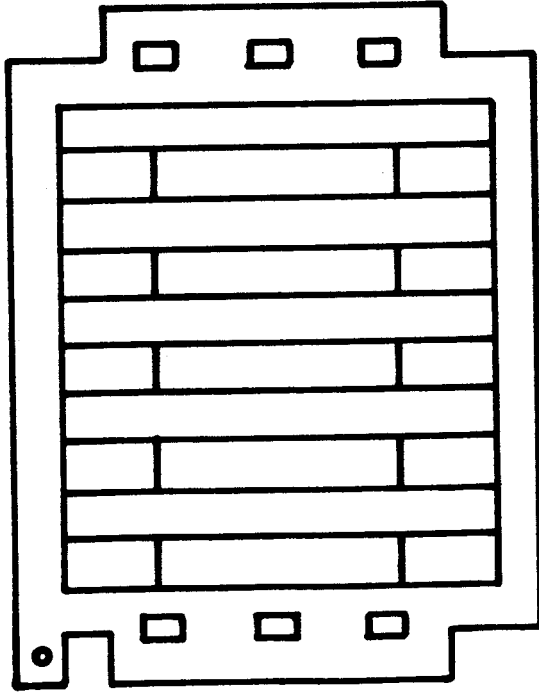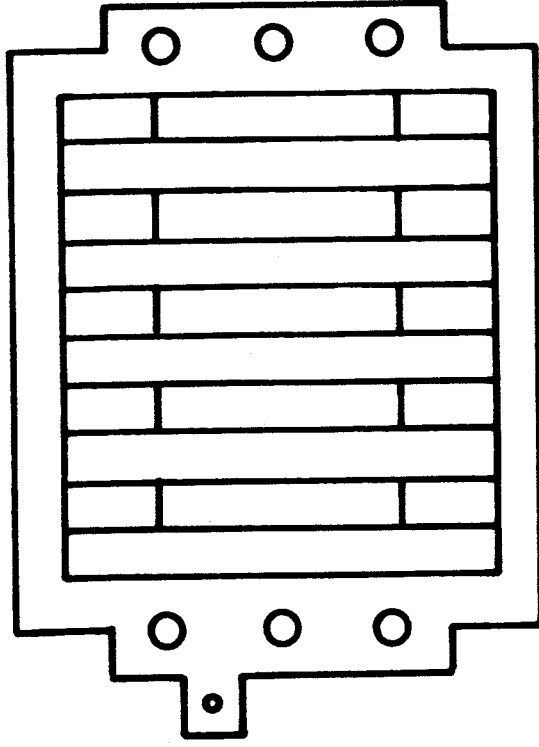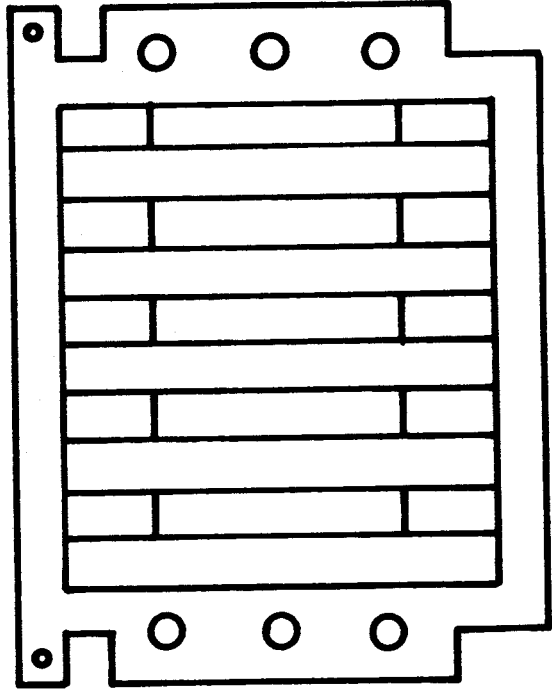
DESIGN #4
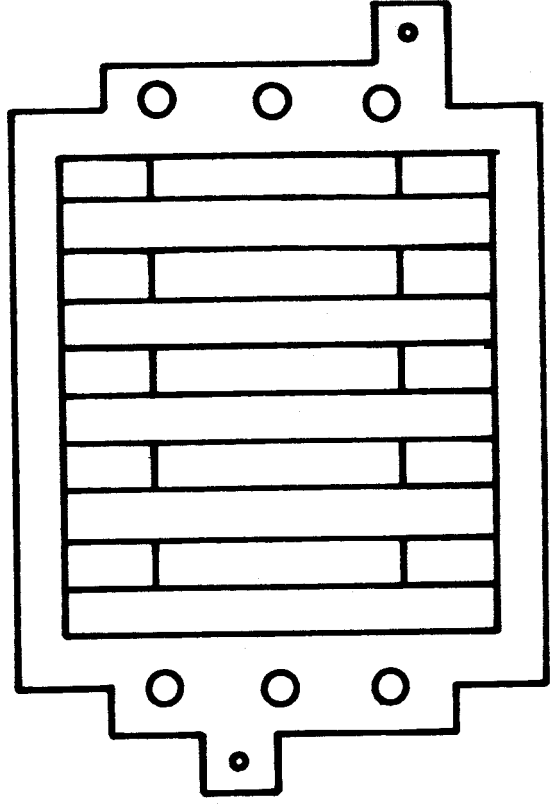
DESIGN #1

DESIGN #3

CELL PLATE DESIGNS

FIGURE 1

FUEL CELL HEAT-UP TRANSIENT
"IN-DUCT" HEATERS

194° MAX.

DUCT TEMP. AT COOLANT ENTRANCE

COOLANT ENTERING DUCT

SECTION #16

SECTION #1

TEMP. ~ °F

ELAPSED TIME, HOURS

FIGURE 2

WATER VAPOR AT PRESSURE P_0 & TEMP. T_0

MOISTURE REMOVAL SUBSYSTEM OF THE FUEL CELL

CONDENSER SEPARATOR UNIT

INLET

OUTLET

FOR THE COOLANT

SEPARATOR

ACCUMULATOR
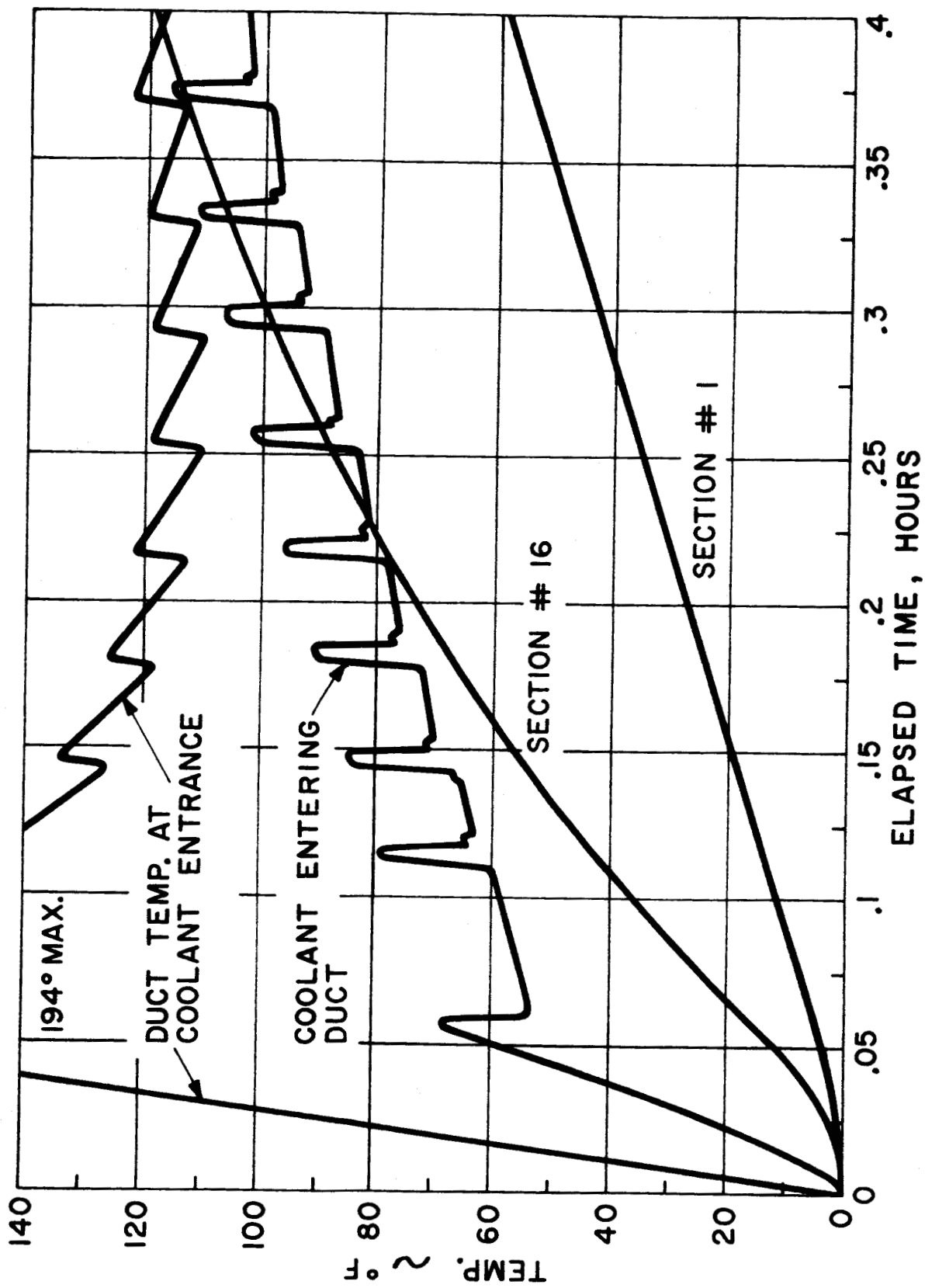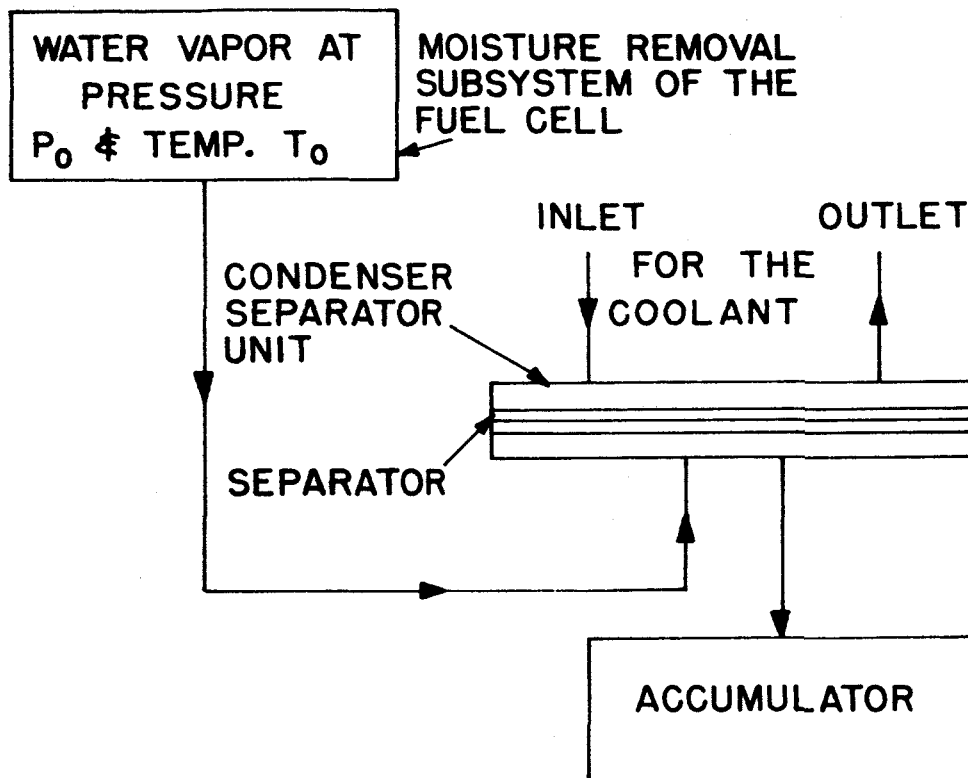
SCHEMATIC DIAGRAM OF A CONDENSER SEPARATOR WATER RECOVERY DEVICE

FIGURE 3

AREA OF HEAT TRANSFER PLATE FOR A 2 LB / HR
(2,138 BTU / HR) SYSTEM

SHAPE OF GROOVES

WATER METHANOL TEMP. RISE = 40° F

WATER METHANOL FLOW RATE = 100 LBS / HR

B = .125, d = .062

.25, .031 & .125, .015

.25, .015

AREA, SQ. FT.

NO. OF GROOVES
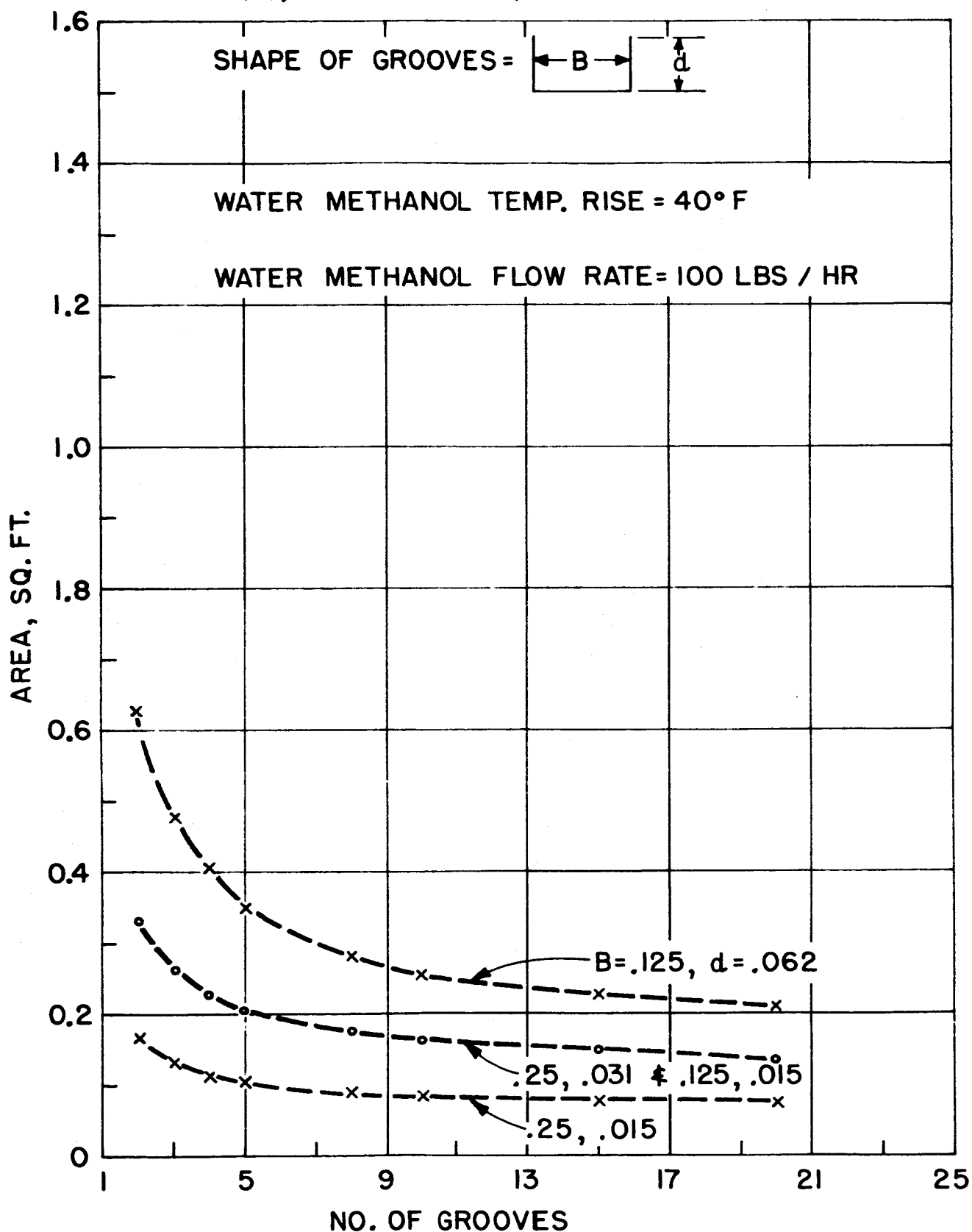
FIGURE 4

PRESSURE DROP IN WATER METHANOL FOR A 2 LB/HR (2,138 BTU/HR) SYSTEM
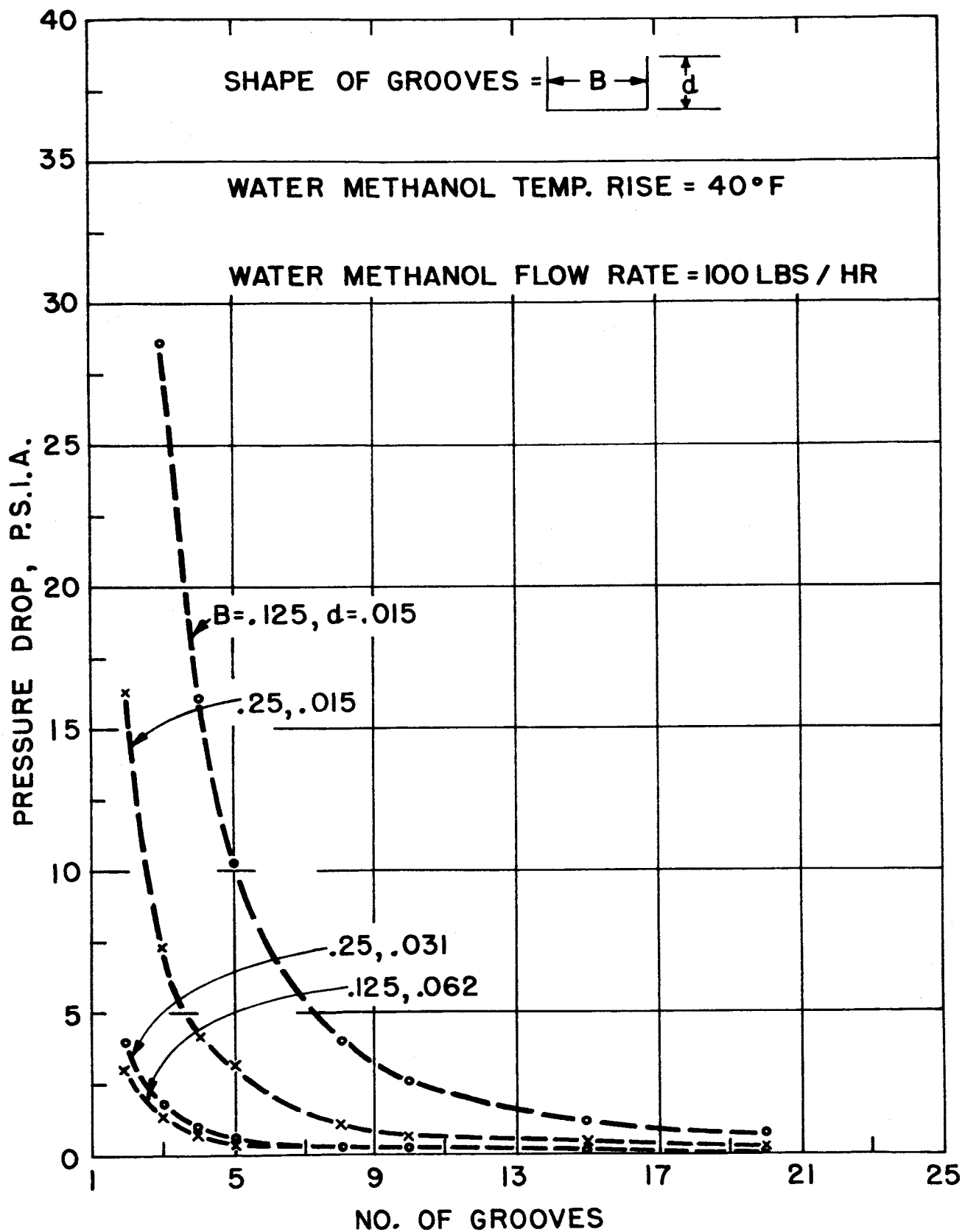
FIGURE 5

FUEL CELL THERMAL TRANSIENT
SEMI-DERIVATIVE CONTROL
2000 WATTS 32 CELLS

FIGURE 6

ELAPSED TIME, HOURS

CELL CENTER TEMP.

COOLANT INLET TEMP.

BYPASS OPEN — BYPASS CLOSED — BYPASS OPEN

FIGURE 7

EFFECT OF PROPORTIONAL SENSITIVITY UPON OFFSET

OFFSET (IN °F)	$K_G = 0$	$K_G = 5$
(b)	19.9	3.67
(c)	89.2	14.6
(d)	0	0
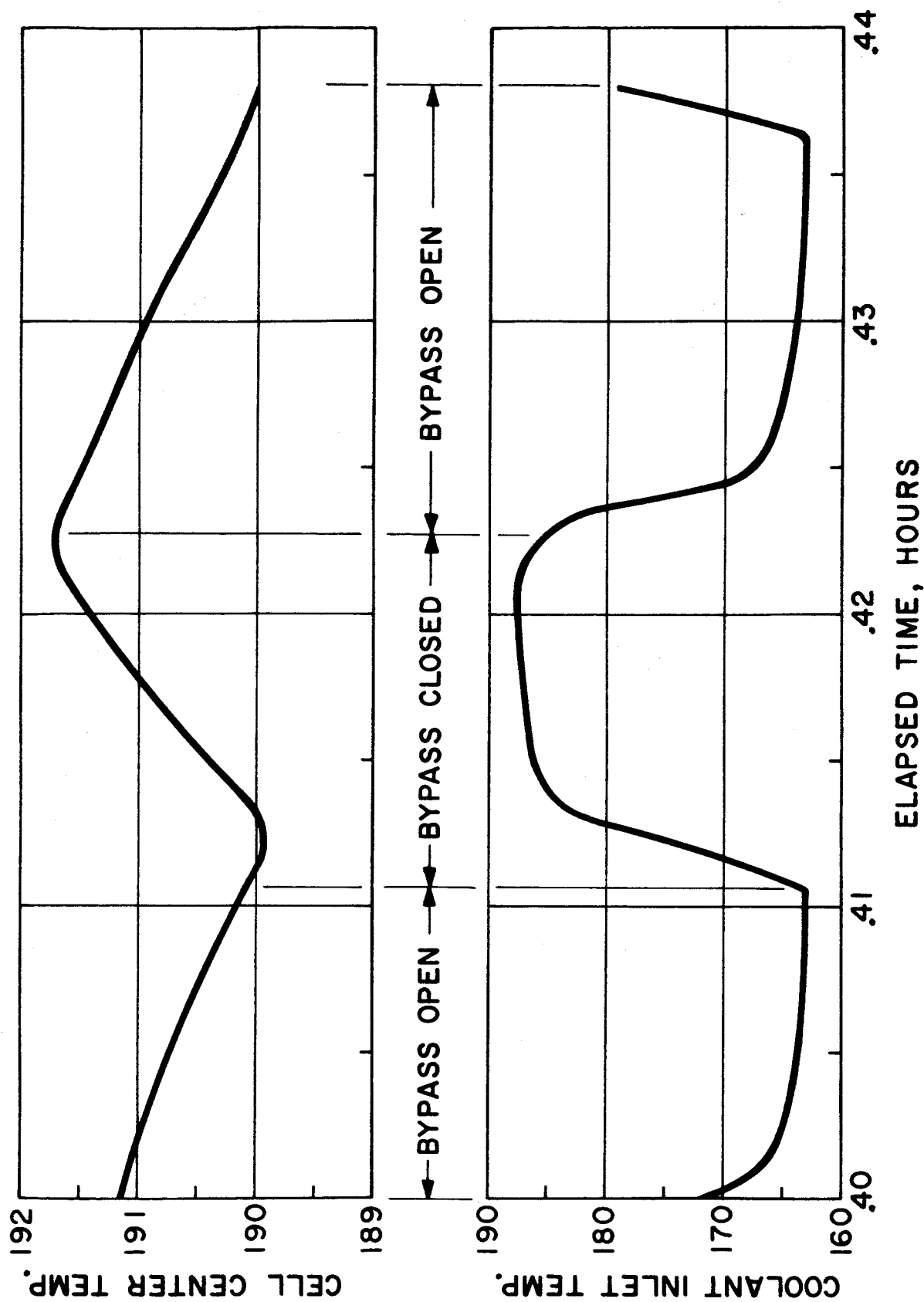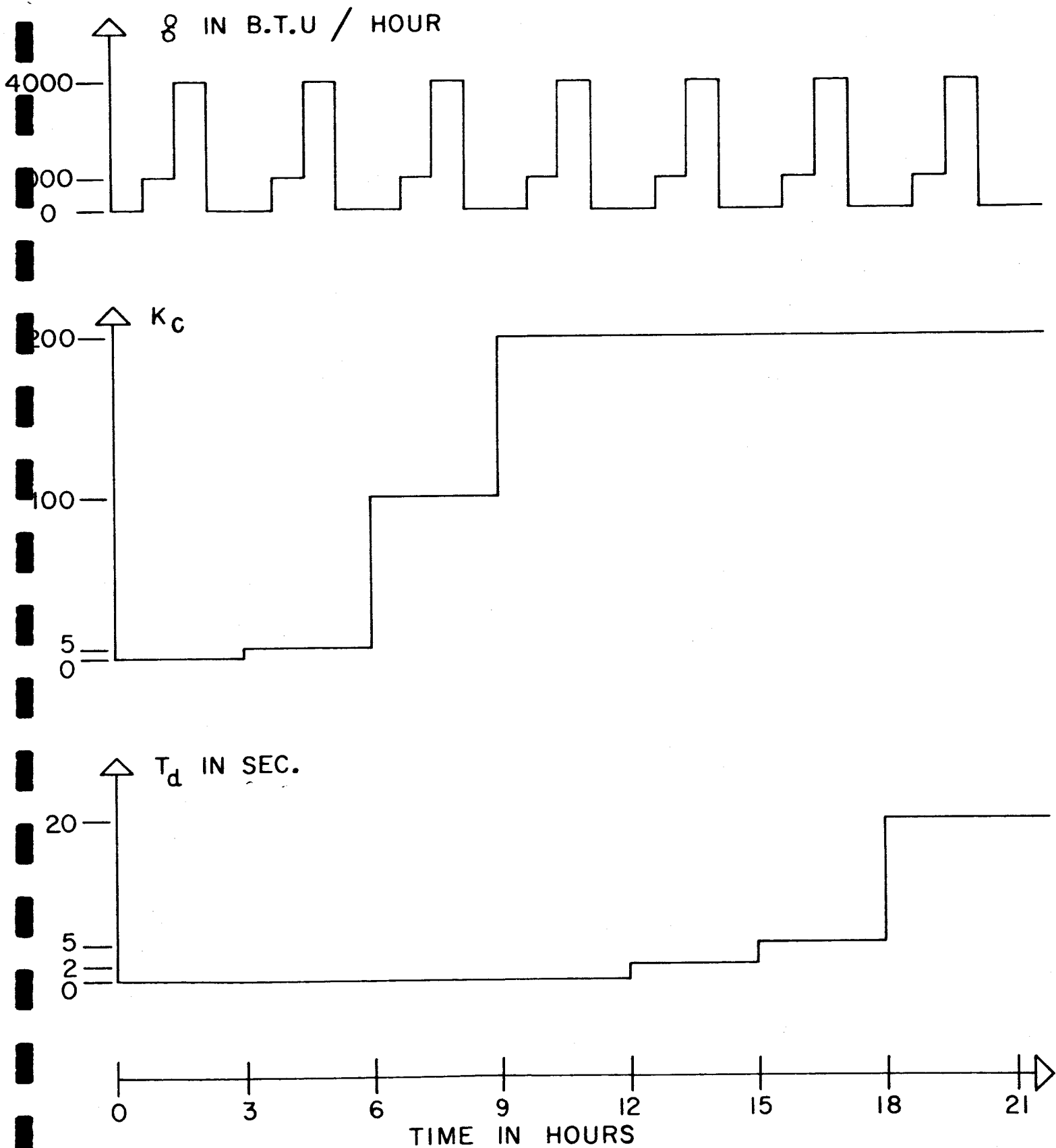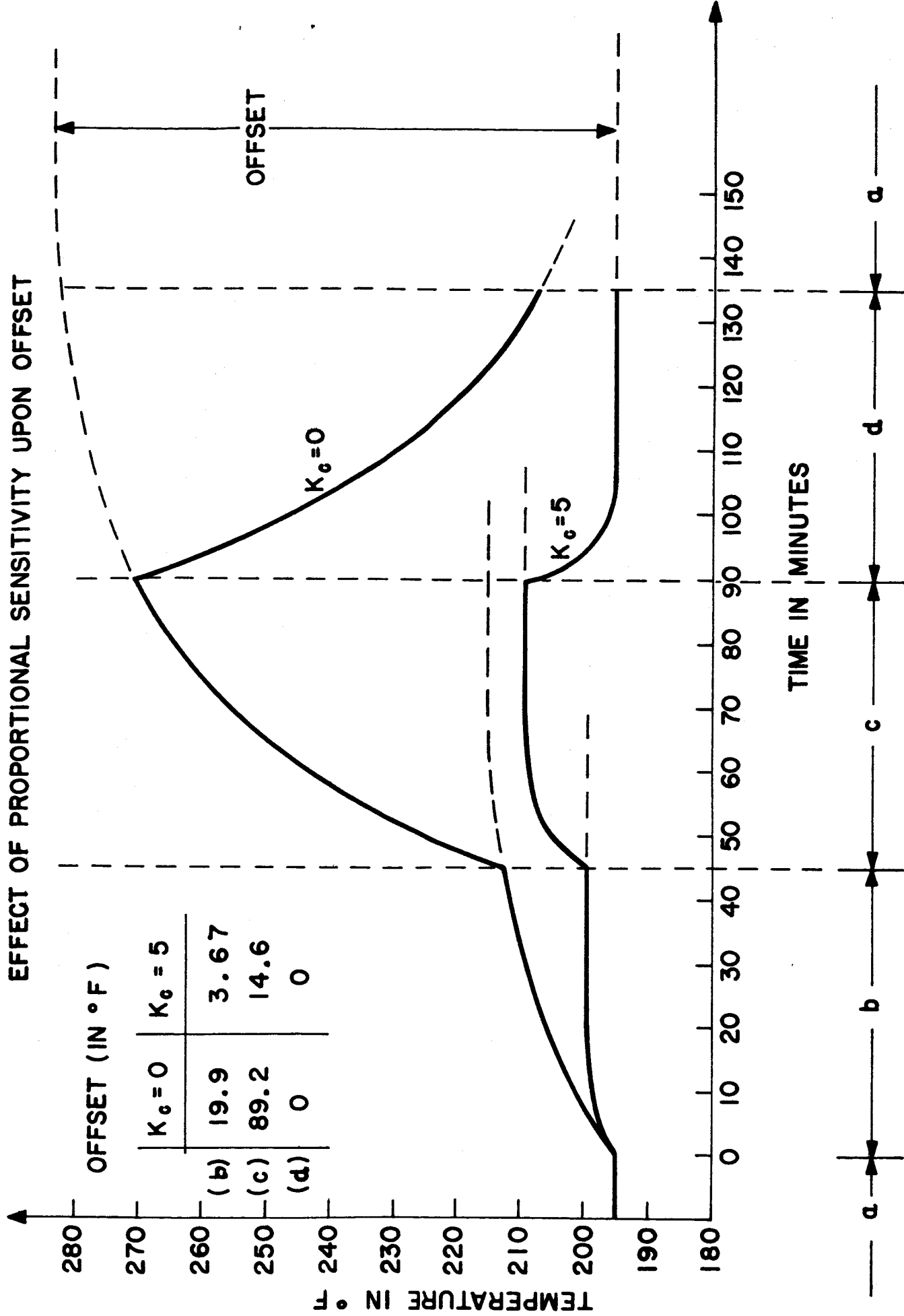
FIGURE 8

ONSET OF INSTABILITY

FIGURE 9

USE OF DERIVATIVE TIME TO PREVENT INSTABILITY

$K_c = 200$
$T_d = 0$

$K_c = 200, T_d = 5$ SEC.

$K_c = 200, T_d = 20$ SEC.
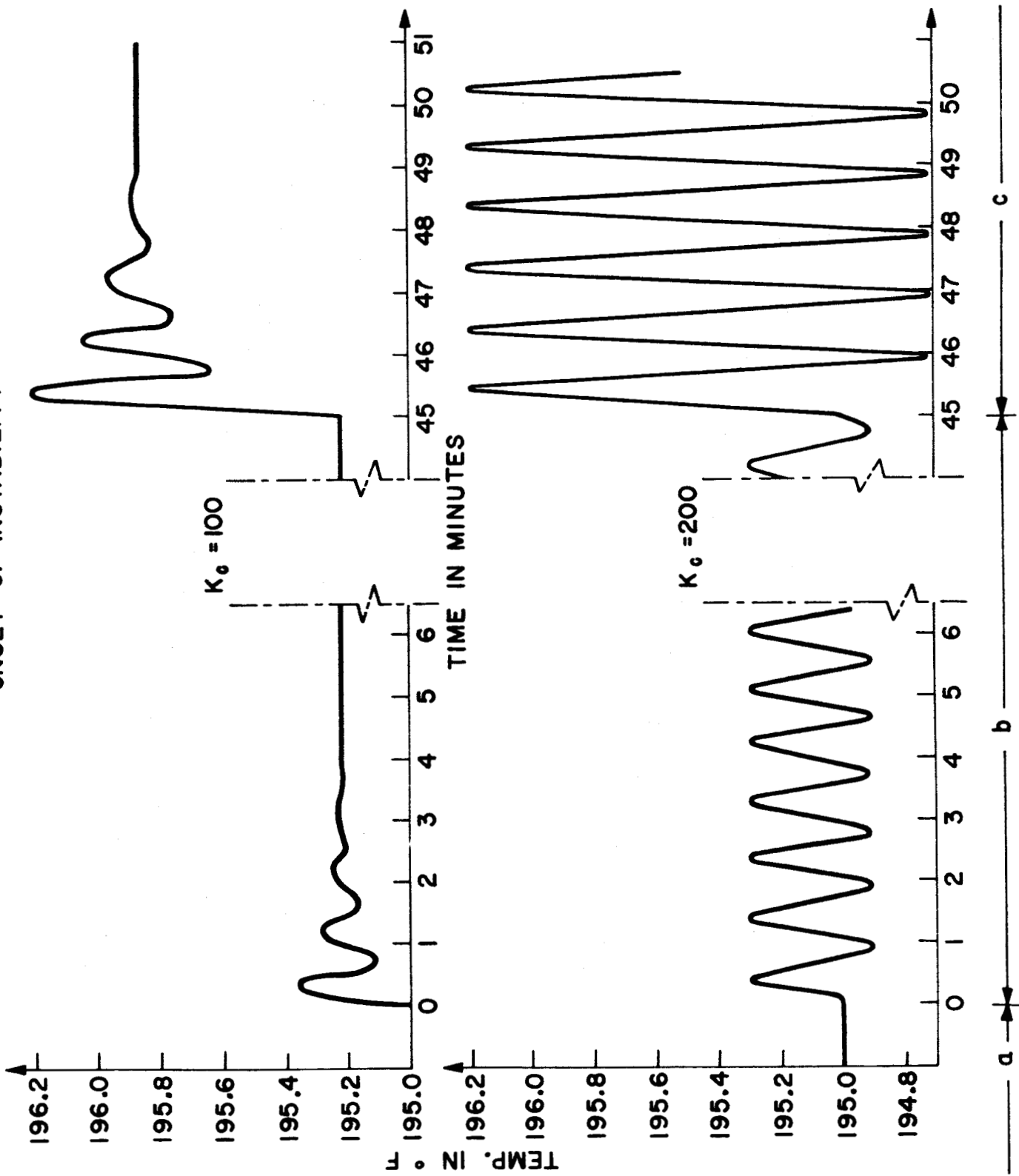
TEMPERATURE IN DEGREES F.

TIME IN MINUTES
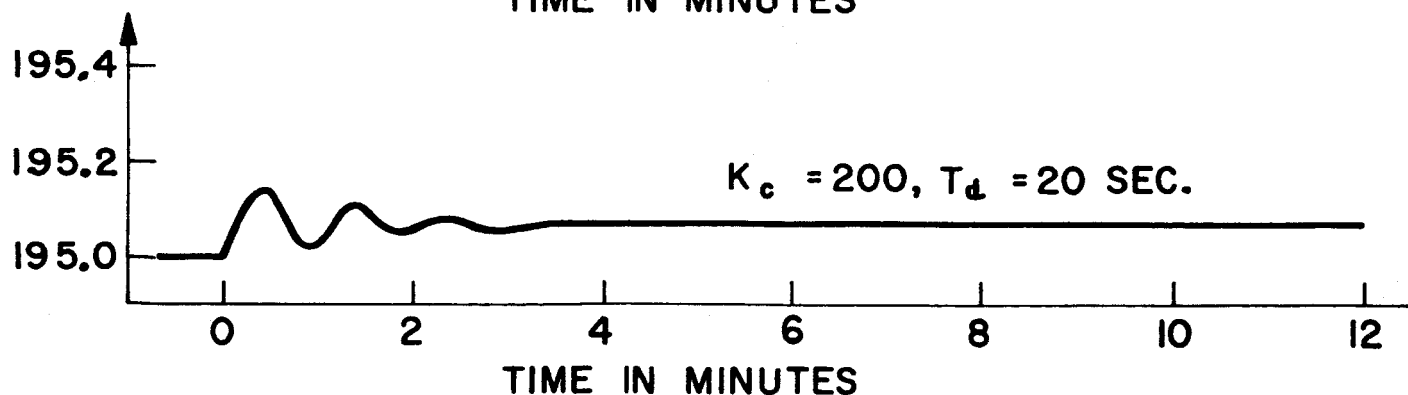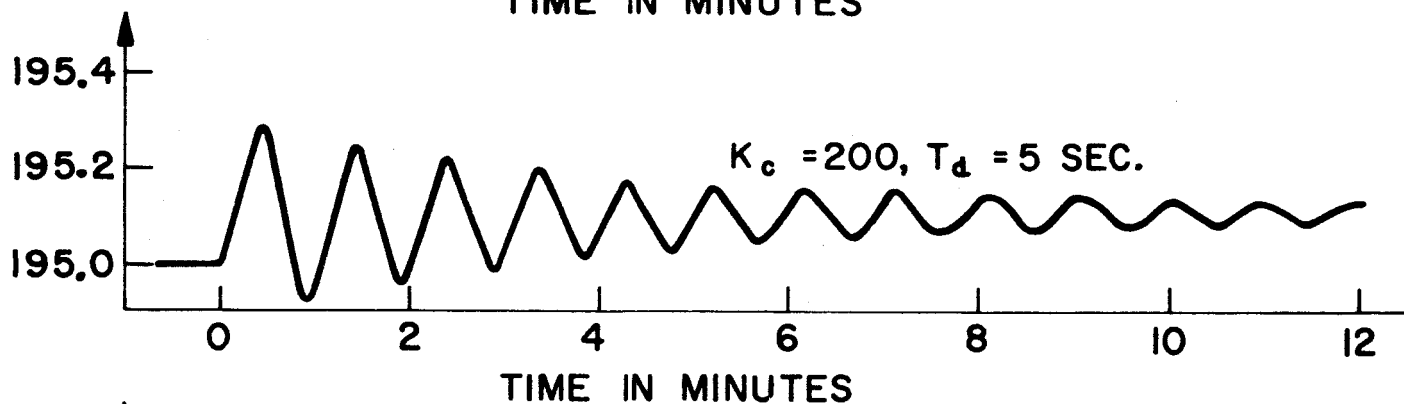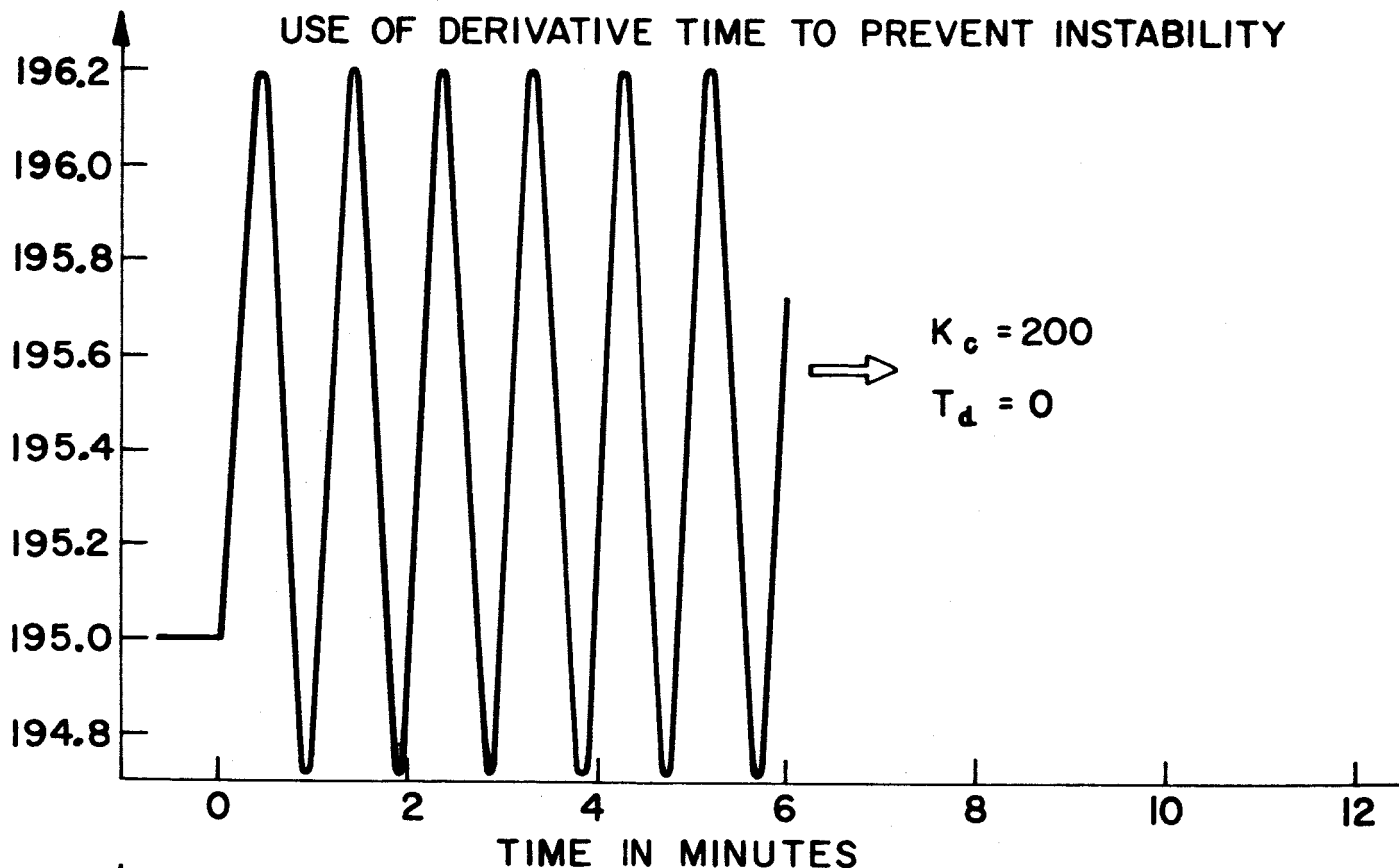
b   c

FIGURE 10

EFFECT OF DEAD TIME

FIGURE II

PRESSURE
RESEVOIR
AT
35 PSIA

⑤

L_1

④

③

$32° F$ $195°F$ L_2

②
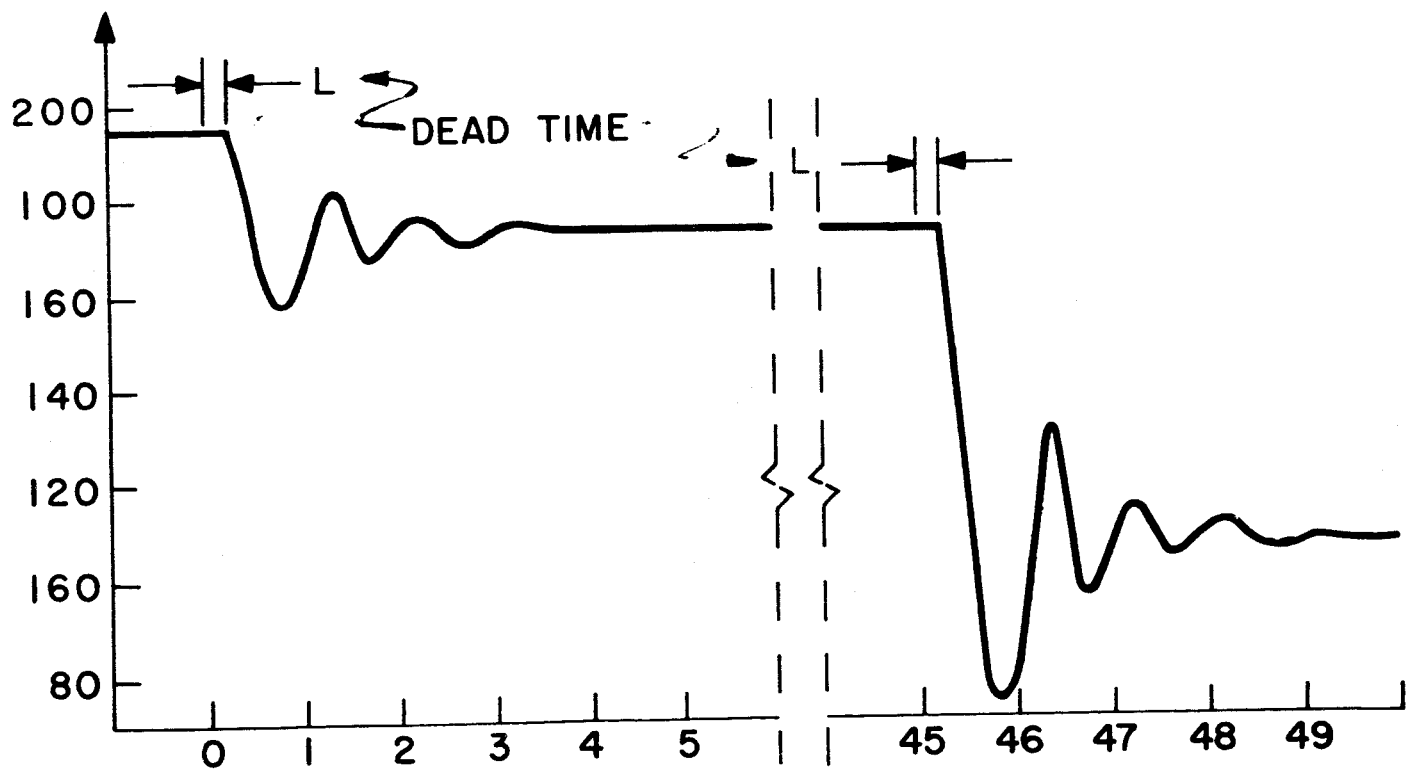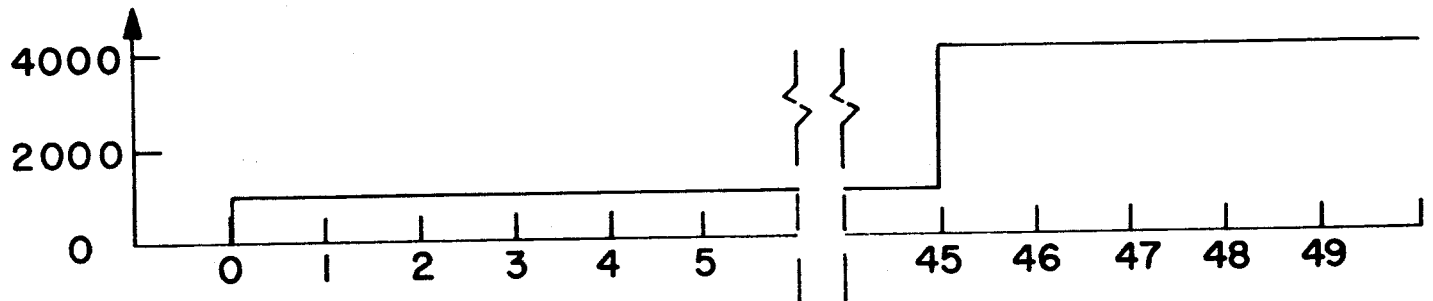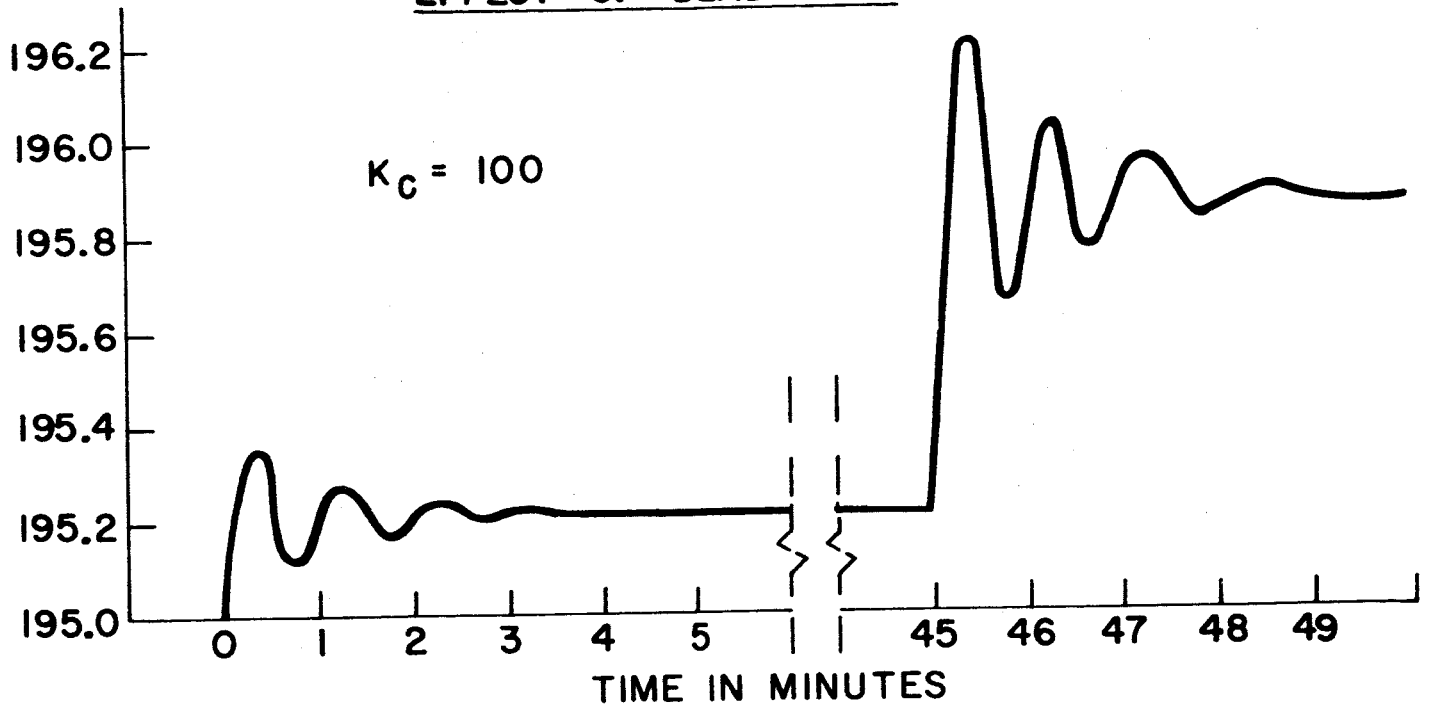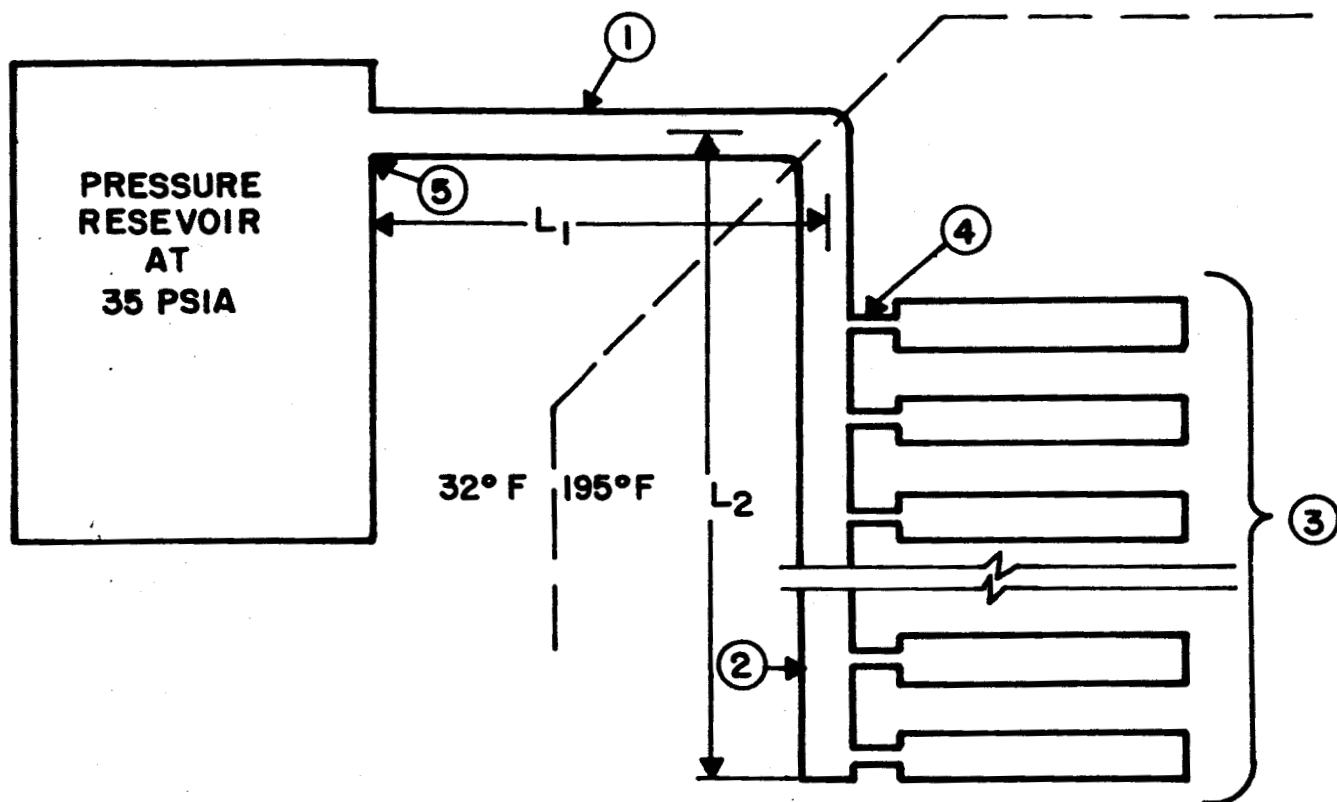
① } INLET TUBING MANIFOLD : HAUING FLOW RESISTANCE R_1 ;
② } GAS CAPACITANCE, C_1 ; INERTIAL INDUCTANCE L .

③ CELL PLATES WITH CAPACITANCE C_2 .

④ SLOT WITH RESISTANCE R_2 .

⑤ ACTUAL POSITION OF CONTROL VALVE .

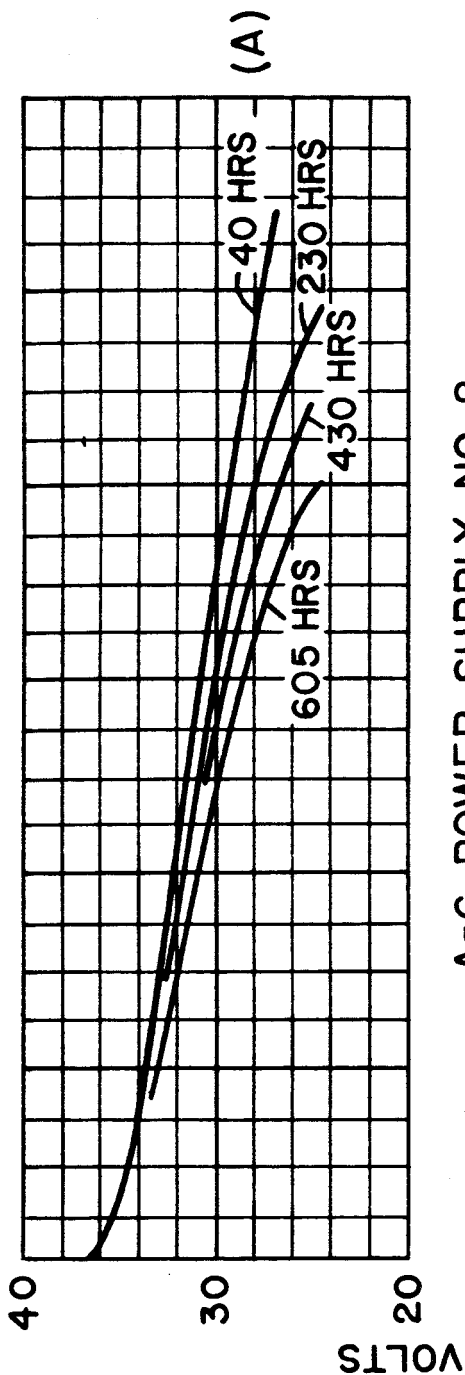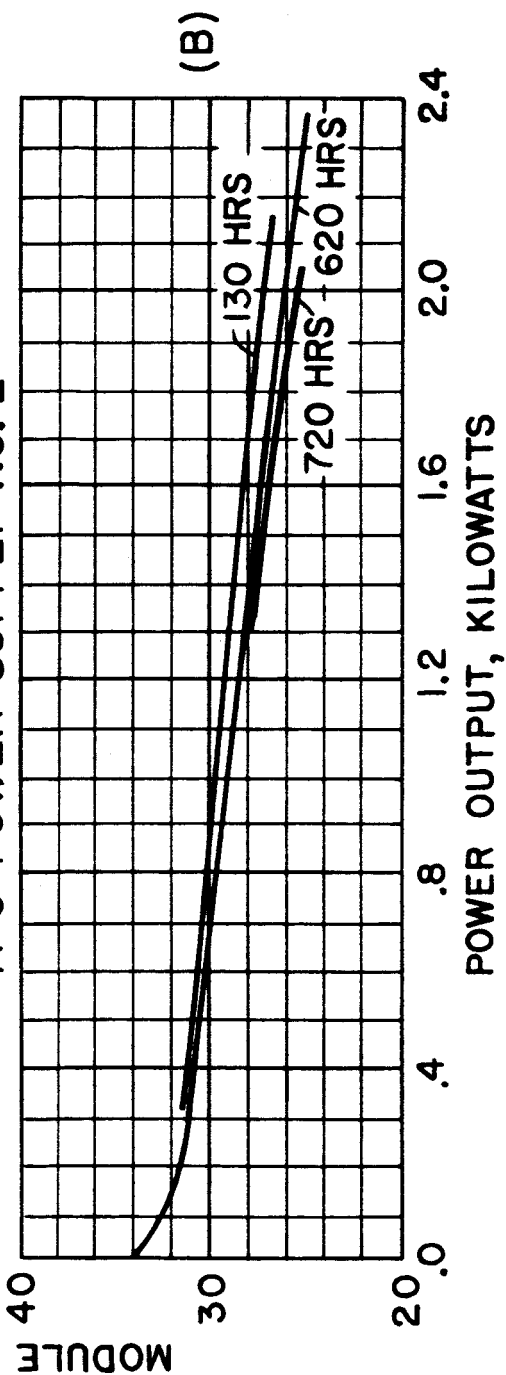MODEL FOR REACTANT GAS SUBSYSTEM

FIGURE 12

PRESSURE RESONANCE IN FUEL CELL SYSTEM
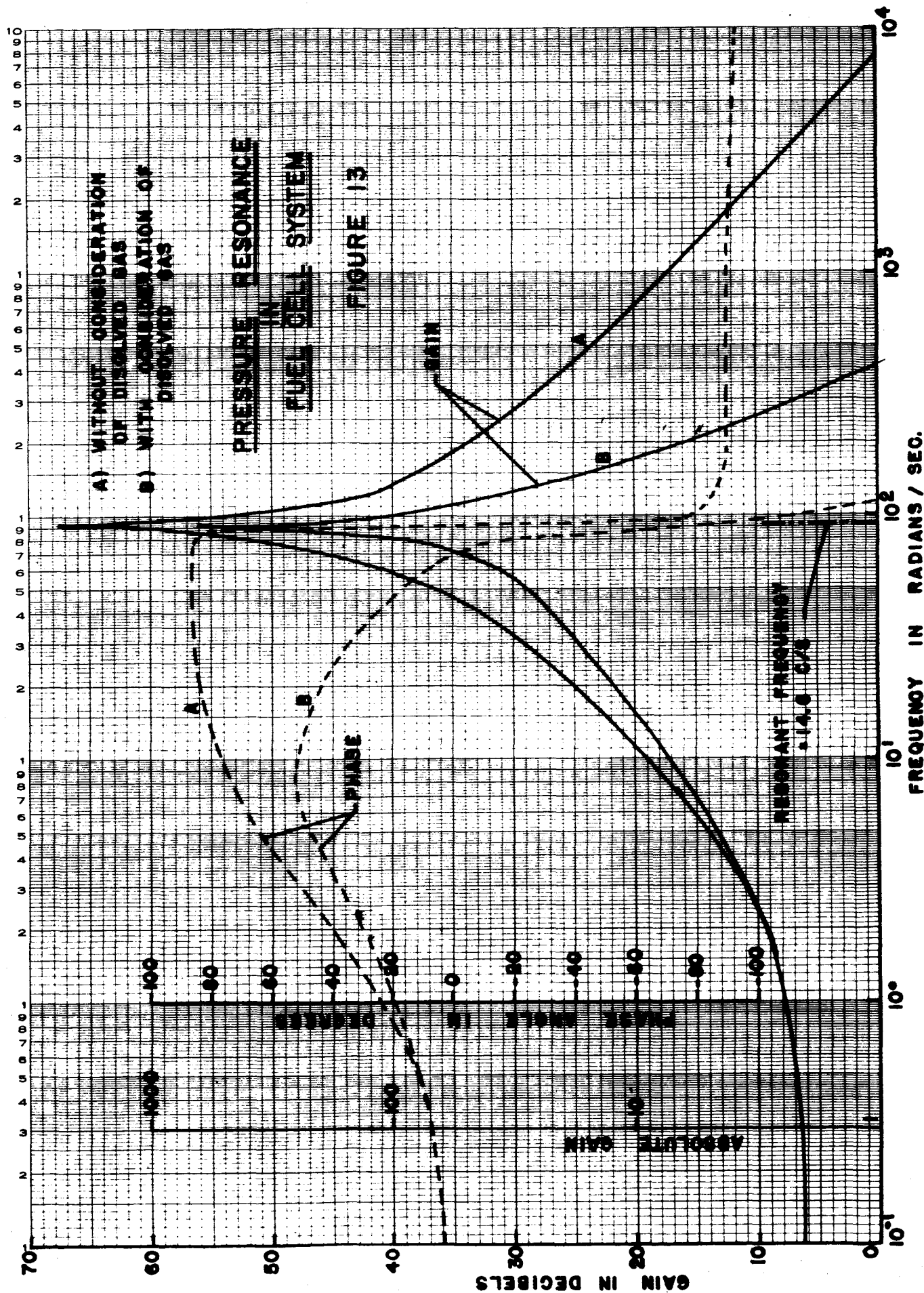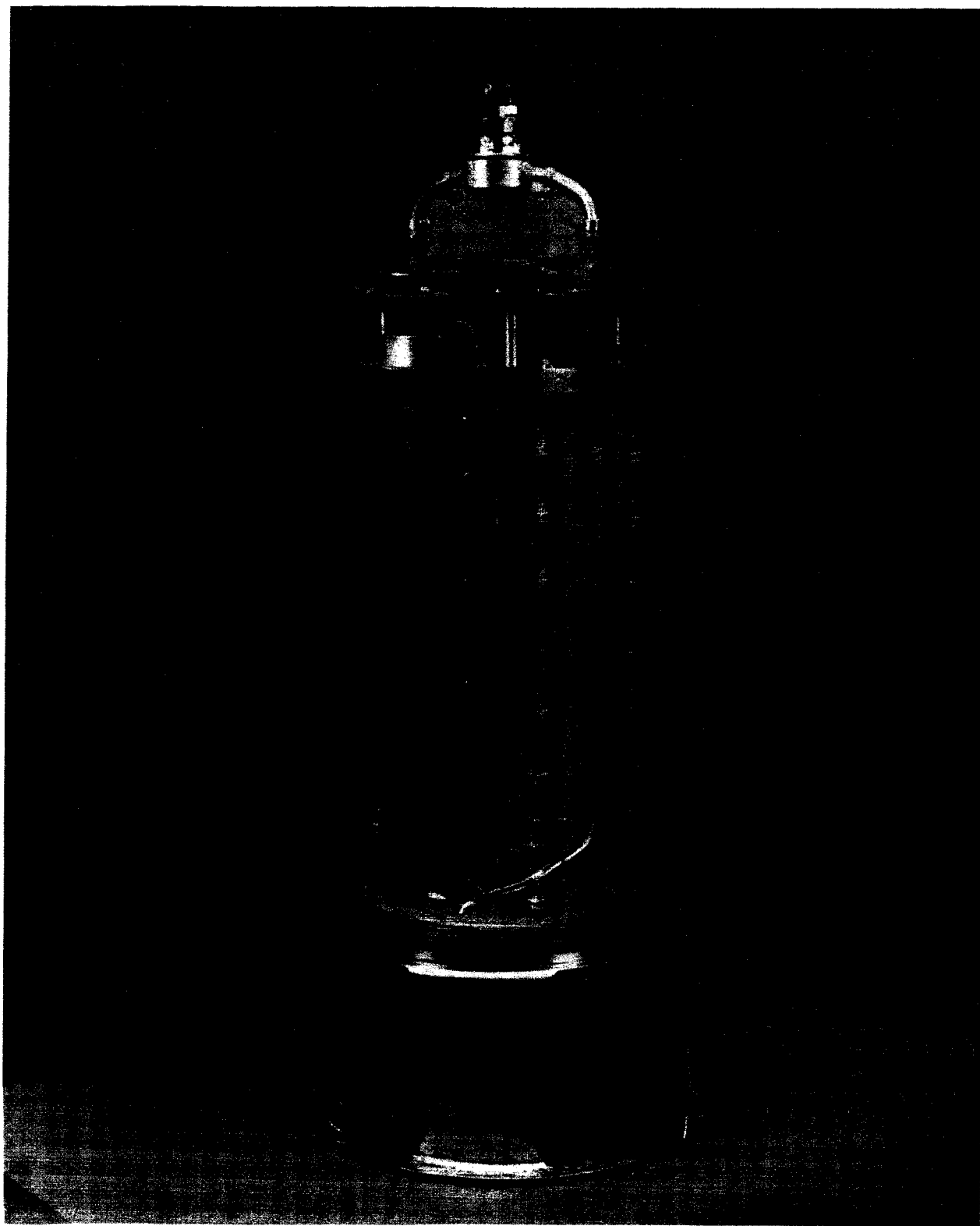
FIGURE 13

Allis-Chalmers Breadboard No. 2 Fuel Cell Module
with Canister Removed

Figure 14

NASA POWER SUPPLY (A)

A-C POWER SUPPLY NO. 2 (B)

40 HRS
230 HRS
430 HRS
605 HRS

130 HRS
720 HRS
620 HRS

MODULE VOLTS

POWER OUTPUT, KILOWATTS

CHARACTERISTICS OF ELECTRICAL
PERFORMANCE

FIGURE 15

VIBRATION CONFIGURATIONS & ACCELEROMETER LOCATIONS

VIBRATION FORCE VECTOR

1. Z ← → Z

LONG SIDE OF STACK PERPENDICULAR TO VIBRATION FORCE VECTOR

ACCELEROMETER LOCATIONS

2. Y ← → Y

SHORT SIDE OF STACK PERPENDICULAR TO VIBRATION FORCE VECTOR

3. X ← → X

LONGITUDINAL AXIS OF STACK PARALLEL TO VIBRATION FORCE VECTOR

HORIZONTAL PLANE
(LISTED IN ORDER OF TESTING)

1. Y

SHORT SIDE OF STACK PERPENDIC — ULAR TO VIBRATION FORCE VECTOR

2. Z

LONG SIDE OF STACK PERPENDICULAR TO VIBRATION FORCE VECTOR
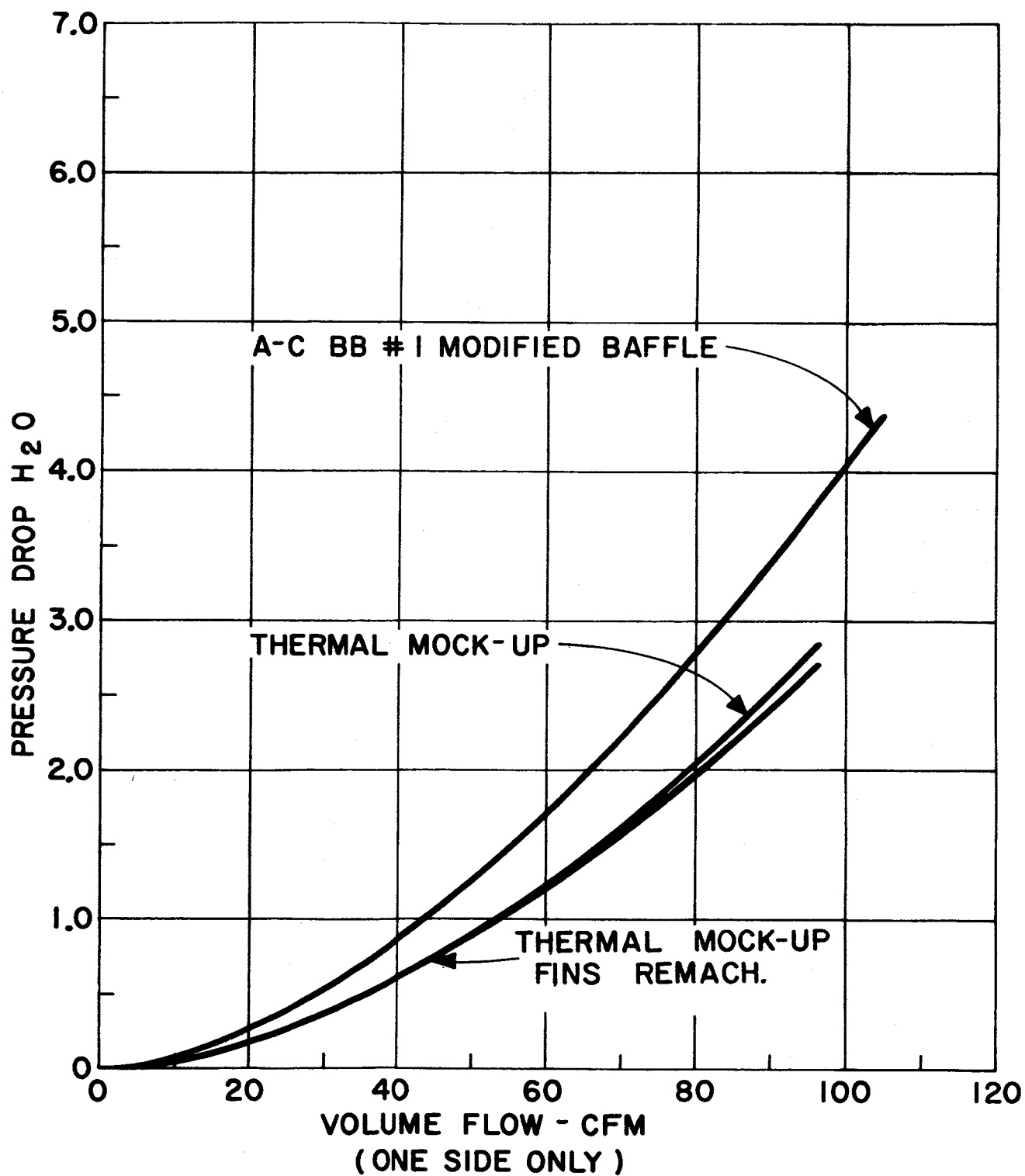
VERTICAL PLANE
(LISTED IN ORDER OF TESTING)

FIGURE 16

SECONDARY COOLANT FLOW RESISTANCE
AIR PRESSURE DROP

FIGURE 17

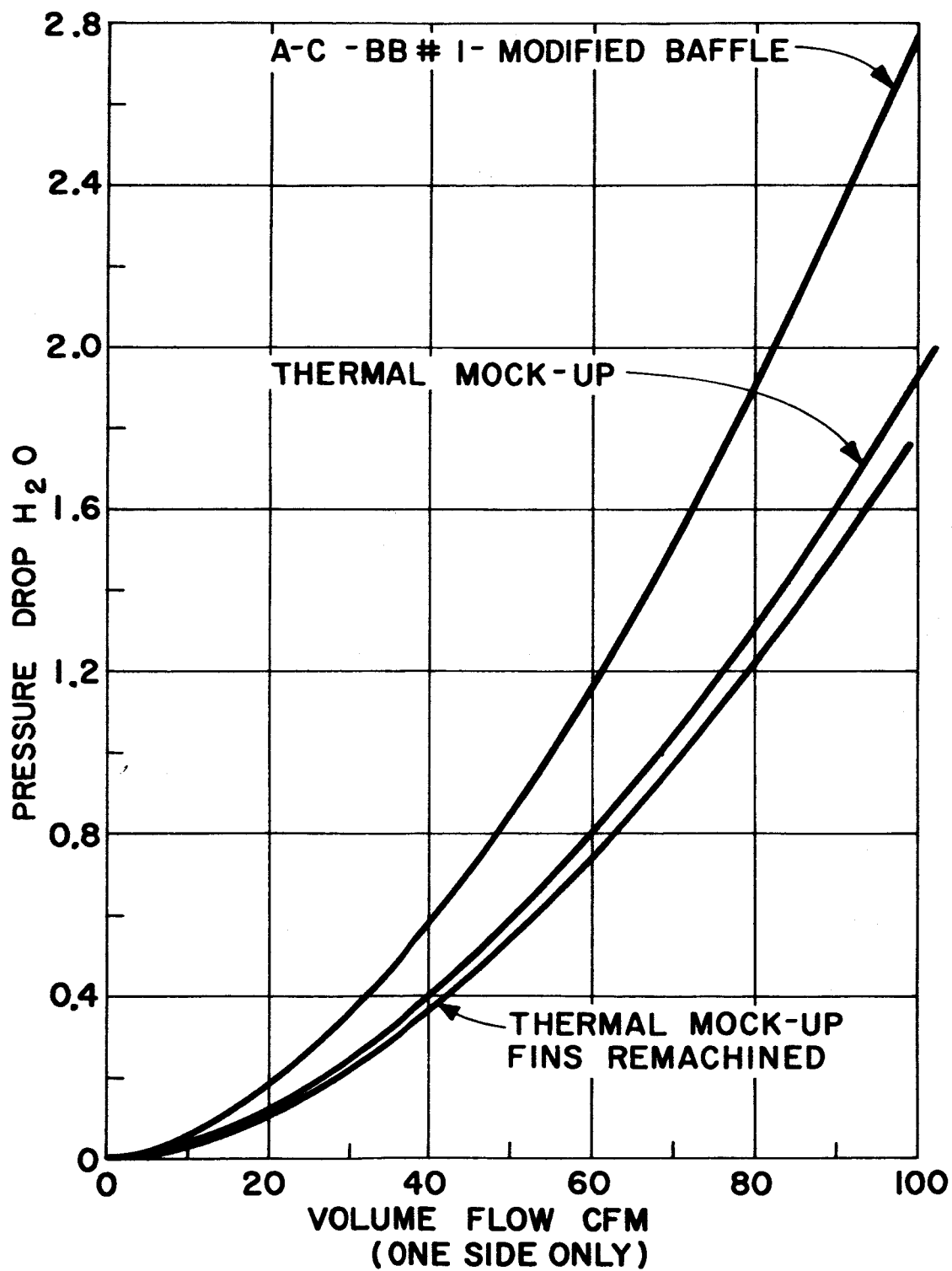# SECONDARY COOLANT FLOW RESISTANCE
HELIUM PRESSURE DROP

A-C -BB # I- MODIFIED BAFFLE

THERMAL MOCK-UP

THERMAL MOCK-UP FINS REMACHINED

PRESSURE DROP H_2O

VOLUME FLOW CFM
(ONE SIDE ONLY)

FIGURE 18

SECONDARY COOLANT FLOW RESISTANCE
HYDROGEN PRESSURE DROP

A-C - BB # I MODIFIED BAFFLES

THERMAL MOCK-UP

THERMAL MOCK-UP
FINS REMACHINED

PRESSURE DROP H₂O

VOLUME FLOW - CFM
(ONE SIDE ONLY)

FIGURE 19

CONDENSER TEST
MAXIMUM WATER FLOW THRU MEMBRANES

STAINLESS STEEL WIRE
CLOTH SUPPORT

WATER COMPLETELY
FILLED INLET & OUTLET
GROOVES

.020 ASBESTOS

.030 ASBESTOS

FLOW cc / min

MEMBRANE DIFFERENTIAL PRESS., Psi
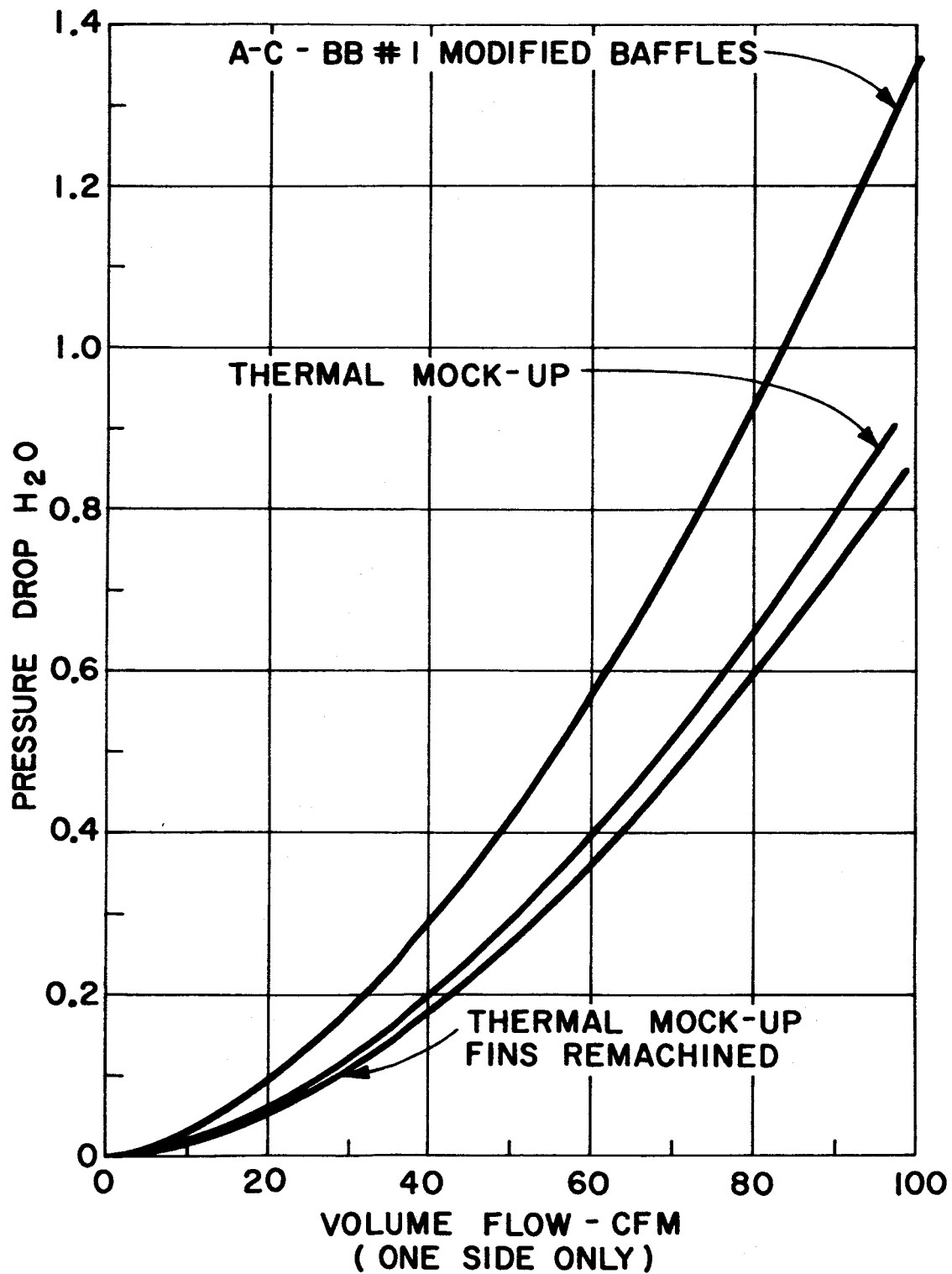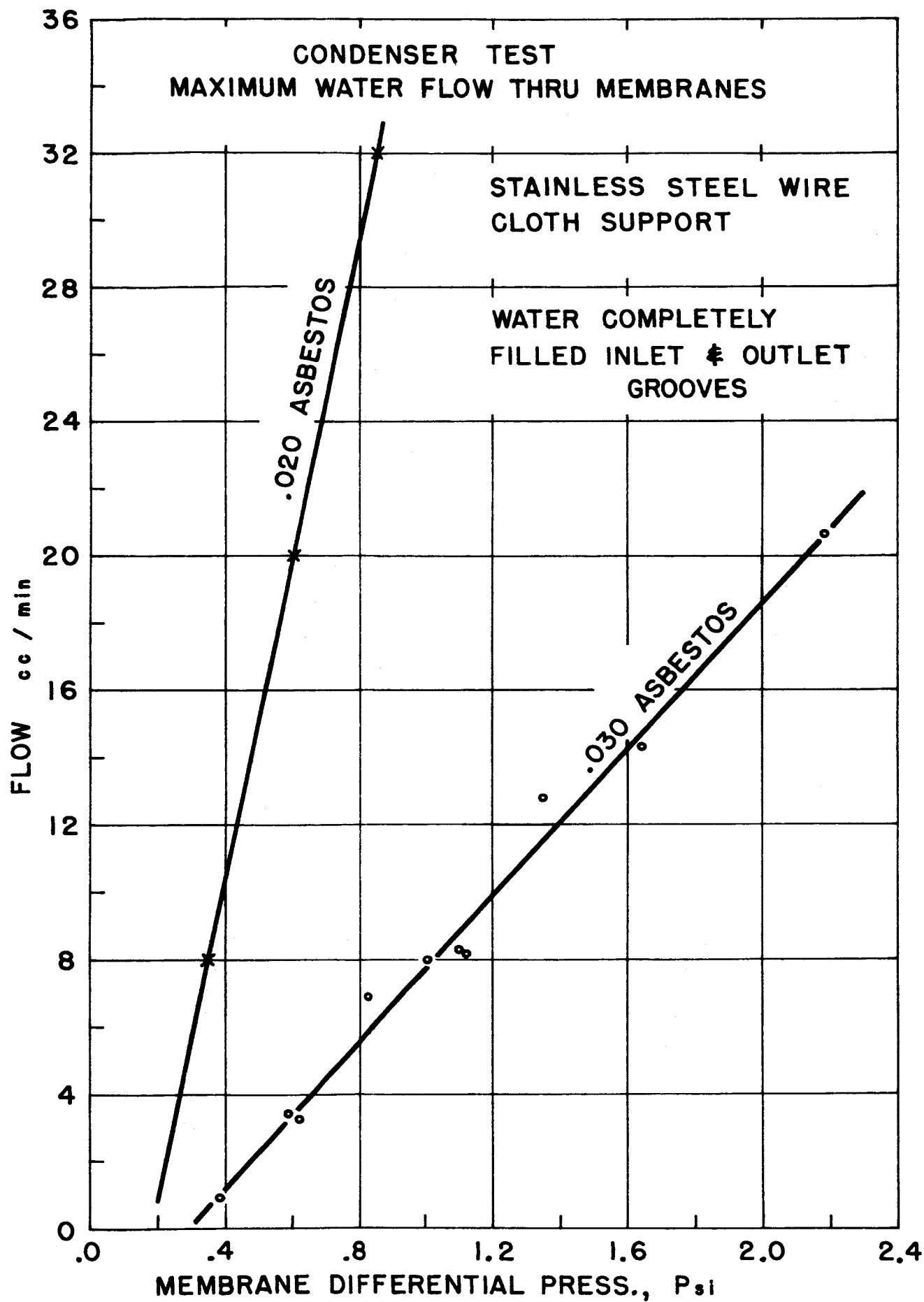
FIGURE 20

WATER RECOVERY SUBSYSTEM
CONDENSER TEST
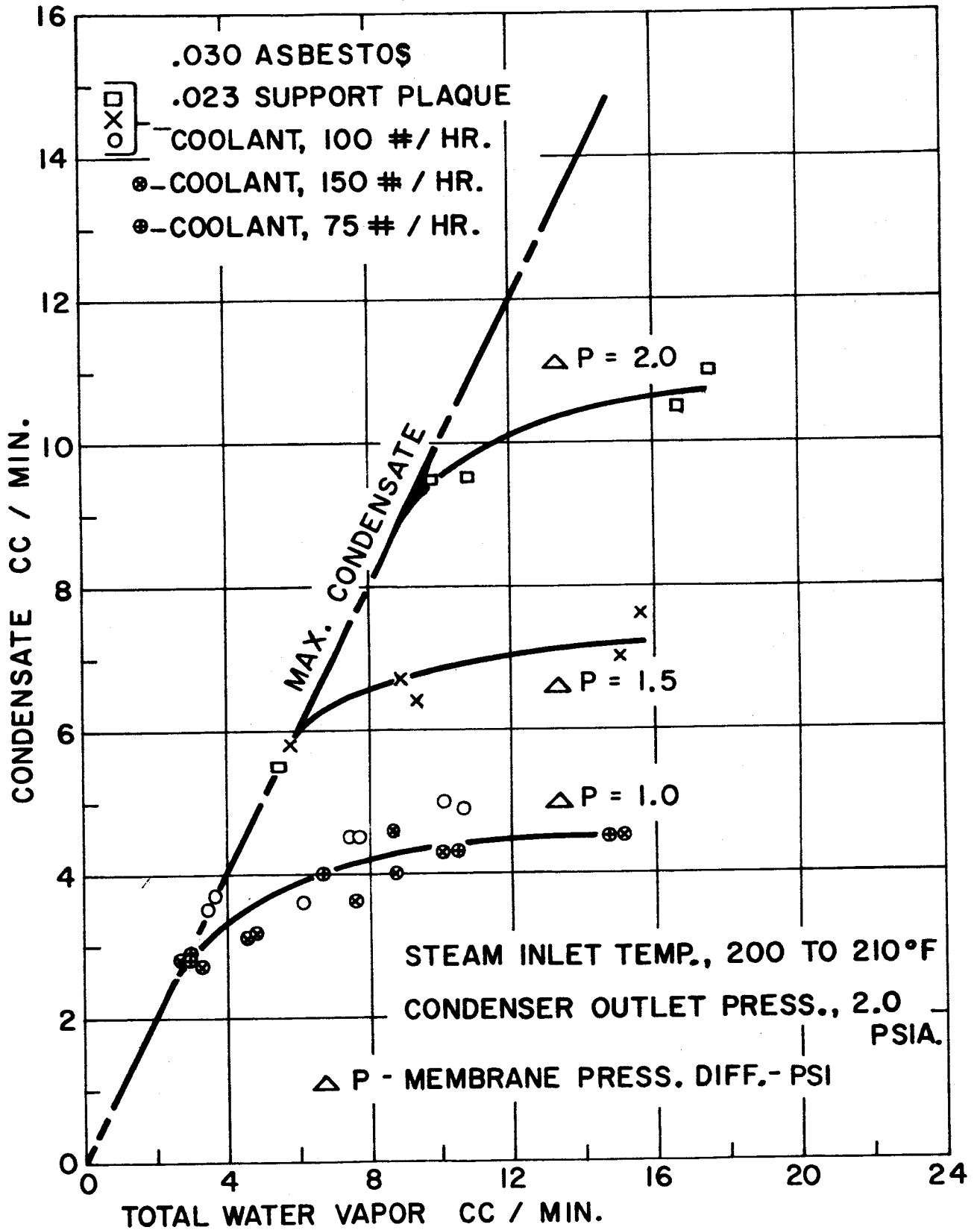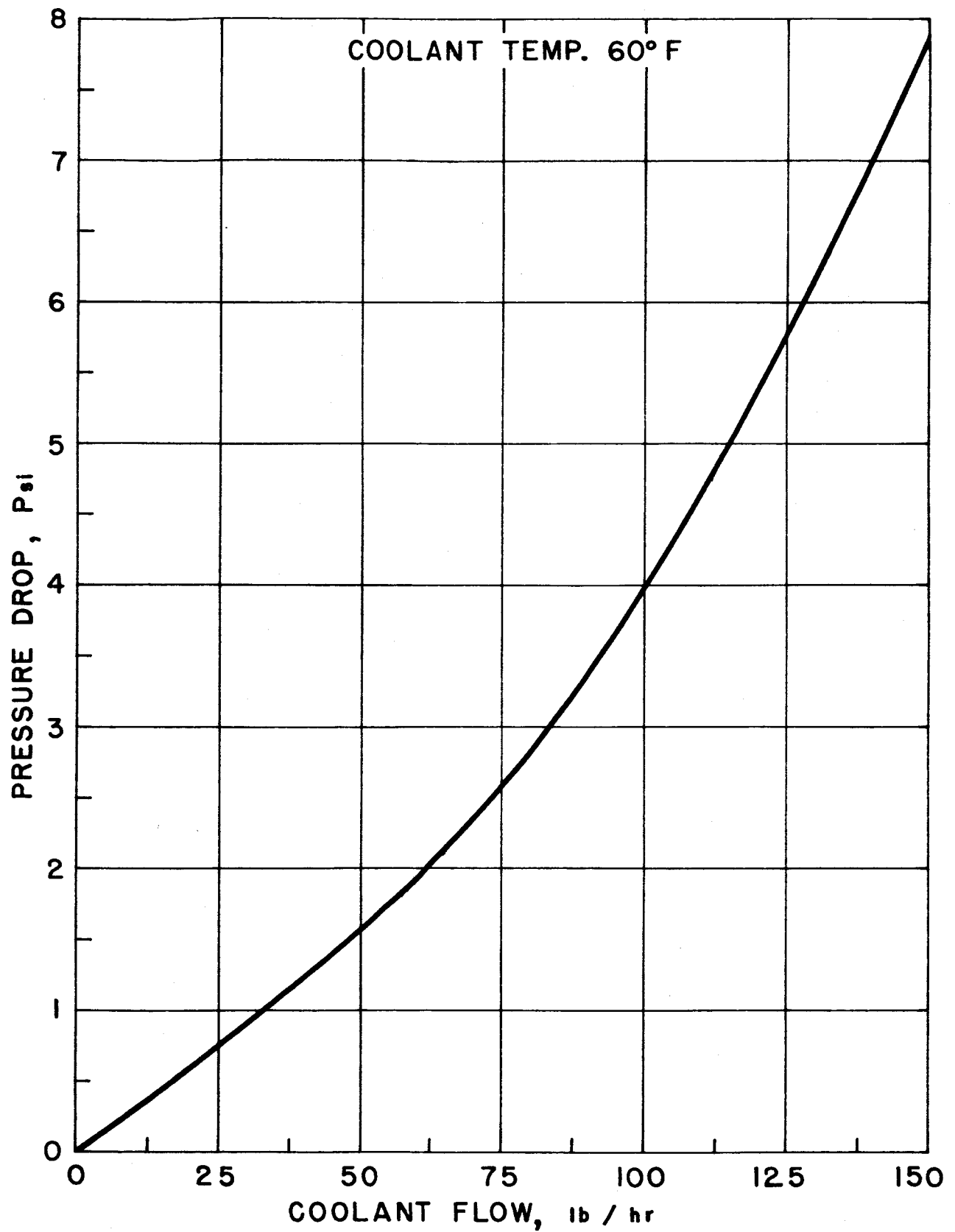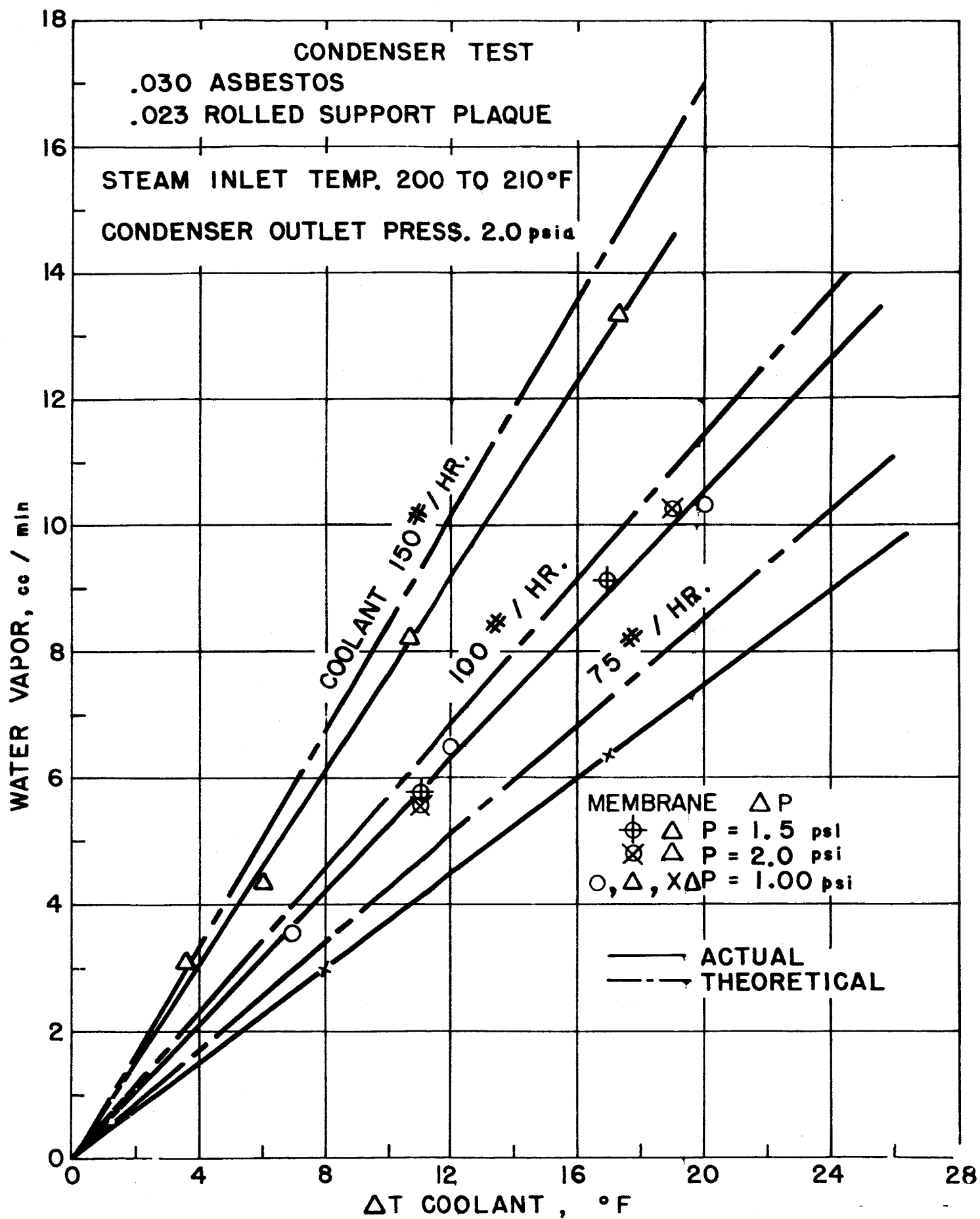
FIGURE 21

CONDENSER TEST
COOLANT PRESSURE DROP

COOLANT TEMP. 60° F
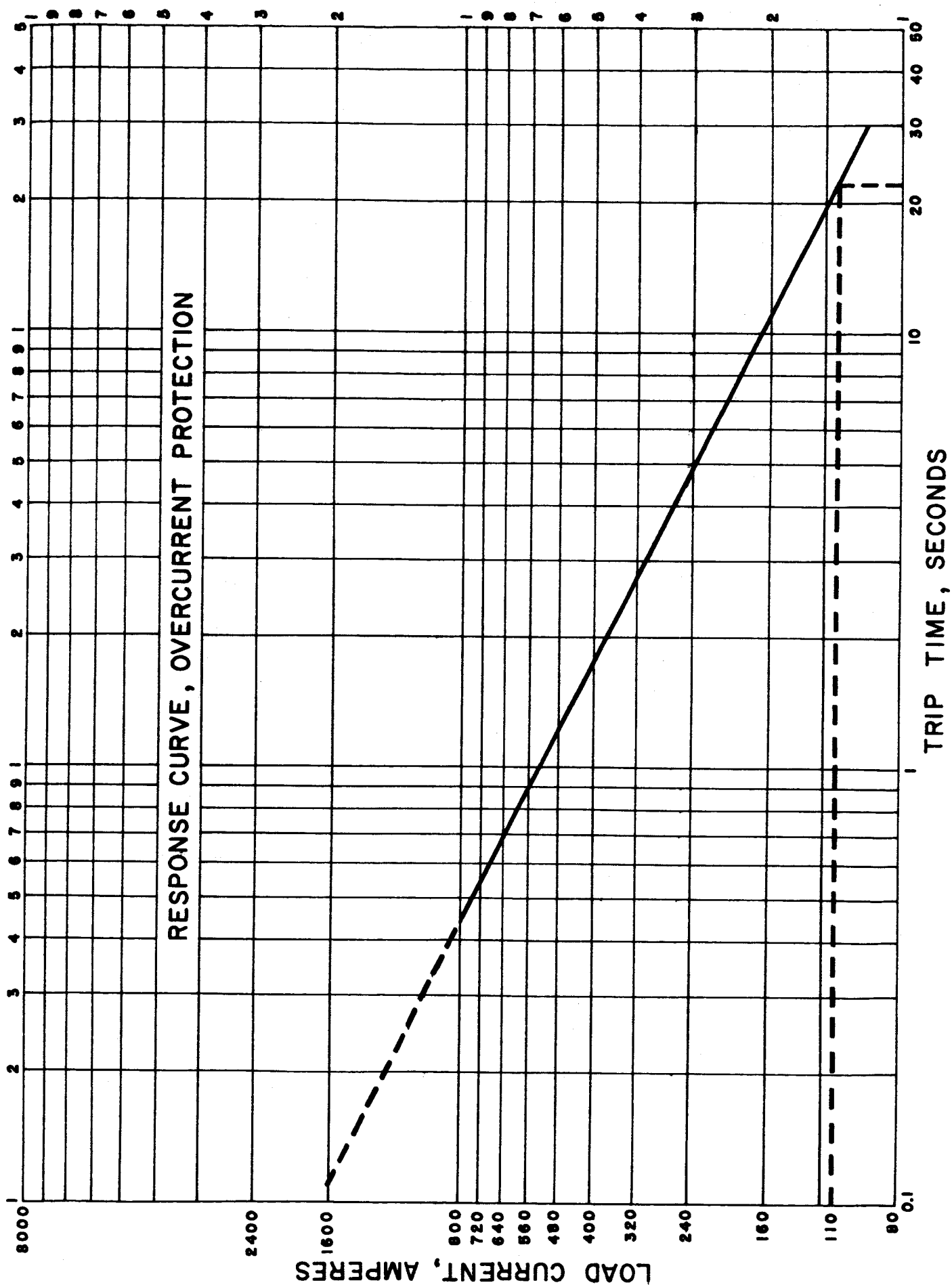
PRESSURE DROP, Psi

COOLANT FLOW, lb / hr

FIGURE 22

FIGURE 23

RESPONSE CURVE, OVERCURRENT PROTECTION

LOAD CURRENT, AMPERES

TRIP TIME, SECONDS

FIGURE 24